1 **<u>Reply to both reviewer</u>**

2 We would like thank both reviewers for reviewing this manuscript. Both reviewers

3 commented fairly and revealed the weak points of our manuscript. We honestly apologize to

4 reviewer 1 for some exaggerated comments in our first reply. However, we have considered

5 the comments from both reviewers carefully and addressed or fully integrated them in the

6 revised version that we have submitted. In addition, we have made small changes throughout

7 the manuscript (text, tables, and figures (marked yellow)) to make it easier for the reader to

8 follow our interpretations of the different trace metal data sets (two separate particulate

9 fractions, the leachable particulate fraction, and the dissolved trace metal fraction). We have

10 also added a section discussing uncertainties associated with our DFe budget in the bloom

11 region north of South Georgia. We are, for instance, well aware that our Fe budget

12 calculations rely heavily on literature values, and that, in the cases of atmospheric dust

13 deposition and horizontal fluxes, were adapted from another region in the Southern Ocean. It

14 was this approach or no budget at all, given the gaps in observational data for the region. Our

15 estimates are not unique in this regard. Almost all ocean DFe budgets rely to some extent on

16 such an approach and also suffer from similar large uncertainties that result. This is now

17 discussed in more detail in section 3.4.6 Budget uncertainties. Furthermore, we included

18 windows comments in the track changed document below to explain made changes and relate

19 them to the reviewers comments.

Methods: -Why were sediment cores collected on the southern
shelf and not the northern shelf? Given that the phytoplankton bloom appears to original
on the northern shelf, and all water column and particle samples were collected
on the northern shelf, this seems like a strange decision. If this was outside of the authors'
control, then this needs to at least be discussed when sediments are compared
to the water column, since one would expect the stronger bloom on the northside to
affect the benthic processing of Fe and Mn, so sediments on the southern shelf may
not be representative of those on the northern shelf.
Answer: Line306ff

-Fecal pellet data are first discussed in section 3.1.3 (for data in Table 4) but without
introducing the methodology for fecal pellet sampling and analysis. They are discussed
again in section 3.2.3, where a reference is to the Schmidt et al papers, but this should
be moved up.
Answer: Line 145ff

Section 3.1.1 -The discussion of particulate fractions in this section is confusing. LPun
is derived from acidified unfiltered seawater and defined in equation 1, but then is
compared to P as if they should be the same, differing only in their sampling methods
(acidified unfiltered seawater vs SAPS sampleâËŸAË˘G Tlines 157-158). However, P is
defined in section 2.2 as the sum of leachable (LP) and refractory (RP) fractions from
the SAPS samples, so one wouldn't expect LPun and P to be the same. I initially read
this section thinking that they were comparing LPun (from acidified unfiltered seawater)
and LP (from acetic acid leach of SAPS samples), which is the more direct comparison
if they want to isolate sampling differences (but still not perfect since acidification to
pH 1.7 with HNO3 is still not the same as a 25% acetic acid leach, but at least more
comparable). This section needs to be clarified. It seems that they have two points in
this section: 1) that pFe and pAl have a refractory component, since LP(un)/P < 100%, and 2) LP(un)
scales with P, so they want to justify using LP(un) for P. For the first point,
it seems that a wholly SAPS-derived assessment of LP/(LP+RP) would be the better
parameter to present, because then there is no confusion of mixing sampling systems,
pore sizes, and leach types. This is done in section 3.2.2 (lines 320-340), which would
make more sense in this section
Answer: Line 179ff and modifications throughout the manuscript

Table 2: are the LPFe, LPAl, LPMn columns derived from the SAPS LP or the bottle
LPun? This should be specified in the caption. The units for the LP are specified
as being in percent. But these values are all very smallâËŸA Ë˘G Tmostly less than
5%, even for Mn, which contradict what was stated in the text in lines 161-163: "The
LPUn corresponded to ca. 63_4% of the PFe, 83_11% of the PAl and 100_10% of
the PMn fractions." Presumably, this discrepancy arises because the Table 2 values
are SAPSbased (LP/P), whereas the values in the text are mixing and matching bottlebased
LPun and SAPS-based totals. Is that correct? If this is the case, then this means
that the bottle-based LPun are much higher than the SAPS-based LPs. One might
expect this to some degree, since the LPun is acidified to a slightly lower pH (_1.7)
and for a lot longer than the SAPS-based LPs (25% acetic acid should have a pH _
2.1), but I wouldn't have expected the difference to be so big. This suggests that the
particle population collected by the SAPS may be a subset of the particles accessed by
the LPun method, and calls into question whether normalizing or comparing the bottle
based LPun by/to the SAPS-based P is appropriate or meaningful. As further detailed
below, I suggest that the authors do not mix bottle-based and SAPS-based parameters
(i.e. they should not report or interpret LPun/P).
Answer: See Table 2

75
76 -Re. lithogenic source of suspended particles: The extremely good correlations of the
77 PFe to PMn and PFe to PAl concentrations (Fig 3a,3b) do support their contention that
78 the particles have a single lithogenic origin (line 197), since biogeochemical processing
79 of the particles would be likely to affect Mn, Fe, and Al differently, and therefore cause
80 more scatter in the data. However, the slopes of their relationships don't support this.
81 The authors base the conclusion that the suspended particles have a lithogenic origin
82 on the slope of the PFe to PMn data (68 mol Fe/mol Mn), which they say agrees
83 well with a typical crustal ratio (they use 60 mol Fe/mol Mn from Wedepohl, which is
84 close to 57 and 50 mol Fe/mol Mn for UCC and BCC crustal averages, respectively,
85 reported by (Taylor and McLennan, 1995)). However, PMn is not usually a good crustal
86 indicator, since Mn-oxides are frequently a large component of marine particulate Mn.
87 For this reason, PAl or PTi are more frequently used to assess how lithogenic the PFe
88 is. However, their PFe to PAl relationship (slope=1.251 mol Fe to mol Al) far exceeds
89 the slope of typical crust (UCC Fe:Al=0.21; BCC Fe:Al=0.41 (Taylor and McLennan,
90 1995)). Since the sediment elemental ratios from the southern shelf (Table 3, line
91 199) are close to these crustal averages, this suggests a fairly large component of the
92 PFe that is in excess of a lithogenic source. One can derive a PMn to PAl ratio from
93 their data=PFe:PAl / PFe:PMn = 0.018 mol Mn/mol Al, which is also greater than typical
94 crustal ratios (UCC Mn:Al=0.0037; BCC Mn:Al=0.0082). So just comparing their slopes
95 to crustal ratios to Al, one would expect there to be a fair amount of nonlithogenic
96 Fe and Mn assuming crustal averages are a reasonable approximation of the local
97 sources (a plausible assumption given that the sediment elemental ratios are close to
98 crustal averages). The conclusion that the suspended particles are primarily lithogenic
99 is therefore not supported by their data.
100 Answer: Line 214ff
101
102 -To rule out data quality issues, the authors should report results from an external standard such as a
103 standard reference material that was run alongside the digestion of the
104 suspended particle leaches/digests. External standards in the supplements were only
105 reported for seawater and for sediments, which used a different digestion procedure
106 than the particles. Was there an external standard measured for the suspended particles
107 to ensure that the digestion method was working accurately?
108 Answer: See Text S1
109
110 Section 3.1.3 -Re. meltwater source of LPunFe: is there a relationship between
111 LPunFe and salinity? A scatter plot of these parameters would be evidence of a meltwater
112 source of LPunFe.
113 Answer: See Fig. S1
114
115 -The authors calculate a vertical supply of DFe to surface mixed layers by assuming a
116 vertical diffusivity and vertical advection (upwelling) used by De Jong et al. 2012 for the
117 region downstream of the Antarctic Peninsula. But later in section 3.4.2, they discuss
118 a study by Tagliabue et al. 2014 modelling DFe supply for South Georgia, in which Ekman
119 *downwelling* (not upwelling!) prevailed, removing DFe from the surface, rather
120 than supplying it. I can appreciate that there's uncertainty in the estimate of vertical advection,
121 but they should probably pick a sign and stick to it!
122 Answer: Line 334ff
123
124 Section 3.3: there are some problems with the proposed flowpaths: -Line 384: I do
125 not understand the proposed advective pathway: the authors reference "Fig. 1; #11/12 via #13 to #14"
126 as a NE-SW transect. First, these stations do not define a NE-SW
127 transect. Second, what is the order of the proposed advective pathway? Is it 13 to 14
128 to 11/12, even though 13 is actually further from the island than 14? Is 13 shallower
129 than 14 (Fig 4) despite being further offshore (Fig 1)?

130   Answer: Line 421ff
131
132   -Presuming that the authors are assuming that #11/12 is the offshore end of the flowpath,
133   this is inconsistent with DMn, which is higher at 11/12 compared to 13 and 14. It's
134   no wonder that they were not able to fit an exponential function to the DFe data (lines
135   409-410). If this isn't an advective flowpath, the good exponential fit to the LPUnFe
136   data may be a coincidence, or at least unrelated to offshore transport. Further, the "exponential
137   decrease" in PFe was based on a 2 point fit! No wonder R2=1! This should
138   be removed.
139   Answer: Line 432ff
140
141   -In the manuscript, an overall vertical loss of DFe of -0.0025 umol DFe/m2/d is assumed
142   (line 465), but in Figure 8, a vertical supply of +0.009 umol DFe/m2/d is indicated.
143   Answer: See Fig.8
144
145   -Given the poor (lack of) constraints on both horizontal and vertical supply of DFe, the
146   suggestion that there is a mismatch in the supply and demand that is filled by advecting
147   biogenic Fe is a nice hypothesis, but rather speculative, both the size of the term, and
148   the nature of it. The size of the flux is not constrained, since they did not have local
149   estimates of horizontal or vertical supply. Re. the nature of their proposed flux: their PFe:PAl ratio
150   from earlier in the manuscript does suggest excess particulate Fe over
151   lithogenic, so this is at least consistent with an available biogenic Fe pool on the shelf,
152   but is also consistent with Fe oxyhydroxides (i.e., authigenic, not biogenic particulate
153   Fe).
154   Answer: See Abstract, Conclusion, Section 3.4.6 and Line 474ff
155

156   **Reviewer2**
157
158   I think that the budget is rather speculative and very uncertain. Many numbers are
159   based on a study (De Jong et al., 2012) performed in a different region, that is the
160   Antarctic Peninsula. This area shares some similarities with the South Georgia Island:
161   a shelf area located in the Southern OCean. However, this does not guarantee
162   that the numbers (diffusive and advectives fluxes) are comparable. Many processes
163   may be significantly different such as tidal mixing, tidal residual current, upwelling (or
164   downwelling) over the shelf, inertial waves, ... As a consequence, I would say that the
165   similarity in terms of geography does not necessarily support the idea that processes
166   should be identical. I understand that better constraining the numbers is a very difficult
167   (if not impossible) task. However, uncertainties should be more extensively discussed.
168   Answer: See section 3.4.6
169
170   The authors suggest that a large part of the offshore supply from the island to the downstream
171   region is sustained by lateral transport of biogenic materials rich in iron (luxury
172   uptake by phytoplankton on the shelf). That's a valid explanation. However, there are
173   some other potential explanations. For instance, labile iron hydroxydes formed on the
174   shelf can also be transported offshore. Iron adsorbed onto biogenic (or non biogenic)
175   particles can also be advected offshore. This should be also discussed by the authors.
176   Over the shelf, the authors state that a large fraction of the iron is being supplied by
177   krills which ingest lithogenic materials (while filtering seawater) and release it as either
178   dissolved iron or as particulate iron within fecal pellets. However, they assume
179   that all of the excreted and egested iron is available as new dissolved iron. This is true if this process
180   solubilizes part of the refractory material which would be otherwise
181   unavailable. This seems to be the case since the LPFe fraction is higher in fecal pellets
182   (_2.5%) than in suspended materials (<1%). This is also true if krills drive a net
183   transport of iron, for instance from the sediment to the open ocean. Again this seems

184   to be true as krills are feeding, at least partly, on sedimentary materials. However,
185   the contribution of this source of food to the total diet of krills is unknown. And thus,
186   the net source of iron due to krills should be uncertain. In other words, it's impossible
187   to quantify the amount of iron that is newly supplied to the system (either by feeding
188   on sediments or by solubilizing an otherwise unavailable iron pool) and the amount of
189   iron that is recycled within the system (grazing on suspended particulate materials and
190   living organisms). This should be better discussed in the manuscript.
191   Answer: Line568ff and Line411ff
192
193   Finally, I have a more specific comment already made by reviewer 1 and that has not
194   been really discussed by the authors. They claim that LPFe exhibits an exponential
195   decrease with the distance from the coast. That's a rather strong assumption knowing
196   that the relationship is derived from three points in one case (stations 14, 13, and 11/12)
197   and from 2 points in the other case (14 and 13). I may have misunderstood something
198   (a plot would help) but 3 or 2 points are not enough to constrain the shape of a function
199   (when this shape is unknown). This explains the very high R2. For instance, 2 points
200   could be fitted by a linear function, a polynomial function, or any continuous function ...
201   Answer: See comments to reviewer1

Mechanisms of dissolved and labile particulate iron supply to shelf waters and phytoplankton blooms off South Georgia, Southern Ocean

Christian Schlosser[1,2,*], Katrin Schmidt[3,4], Alfred Aquilina[1], William B. Homoky[1,5], Maxi Castrillejo[1,6], Rachel A. Mills[1], Matthew D. Patey[1], Sophie Fielding[3], Angus Atkinson[7], and Eric P. Achterberg[1,2]

[1] Ocean and Earth Science, National Oceanography Centre Southampton, University of Southampton, SO14 3ZH Southampton, United Kingdom

[2] GEOMAR Helmholtz Centre for Ocean Research, Wischhofstr. 1-3, 24148 Kiel, Germany

[3] British Antarctic Survey, CB3 0ET Cambridge, United Kingdom

[4] School of Geography, Earth and Environmental Sciences, University of Plymouth, PL4 8AA Plymouth, United Kingdom

[5] Department of Earth Sciences, University of Oxford, OX1 3AN Oxford, United Kingdom

[6] Institut de Ciència i Tecnologia Ambientals & Departament de Física, Universitat Autònoma de Barcelona, 08193 Bellaterra, Spain

[7] Plymouth Marine Laboratory, Prospect Place, The Hoe, PL1 3DH Plymouth, United Kingdom

Kommentar [SC1]: Author changed affiliation

For submission to Biogeosciences

* Corresponding author Christian Schlosser (Email: cschlosser@geomar.de, Phone: 0049 (0) 431 600 1297)

Abstract (369 words)

The island of South Georgia is situated in the iron (Fe) depleted Antarctic Circumpolar Current of the Southern Ocean. Iron emanating from its shelf system fuels large phytoplankton blooms downstream of the island, but the actual supply mechanisms are unclear. To address this, we present an inventory of Fe, manganese (Mn) and aluminium (Al) in shelf sediments, pore waters and the water column in the vicinity of South Georgia, alongside data on zooplankton-mediated Fe cycling processes, and provide estimates of the relative dissolved Fe (DFe) fluxes from these sources. The seafloor sediments were the main particulate Fe source to shelf bottom waters as indicated by the similar Fe/Mn and Fe/Al ratios for shelf sediments and suspended particles in the water column. Less than 1% of the total particulate Fe pool was leachable surface adsorbed (labile) Fe, and therefore potentially available to organisms. Pore waters formed the primary DFe source to shelf bottom waters supplying $0.1 - 44$ µmol DFe m^{-2} d^{-1}. However, we estimate that only 0.41 ± 0.26 µmol DFe m^{-2} d^{-1} was transferred to the surface mixed layer by vertical diffusive and advective mixing. Other trace metal sources to surface waters included glacial flour released by melting glaciers and via zooplankton egestion and excretion processes. On average 6.5 ± 8.2 µmol m^{-2} d^{-1} of labile particulate Fe was supplied to the surface mixed layer via faecal pellets formed by Antarctic krill (*Euphausia superba*), with a further 1.1 ± 2.2 µmol DFe m^{-2} d^{-1} released directly by the krill. The faecal pellets released by krill included seafloor-derived lithogenic material and settled algal debris, in addition to freshly ingested suspended phytoplankton cells.

The Fe requirement of the phytoplankton blooms ~1,250 km downstream of South Georgia was estimated at 0.33 ± 0.11 µmol m^{-2} d^{-1}, with the DFe supply by horizontal/vertical mixing, deep winter mixing and aeolian dust estimated as ~0.12 µmol m^{-2} d^{-1}. We hypothesize that a substantial contribution of DFe was provided through recycling of biogenically stored Fe following luxury Fe uptake by phytoplankton on the Fe-rich shelf. This process would allow Fe to be retained in the surface mixed layer of waters downstream of South Georgia through continuous recycling and biological uptake, supplying the large downstream phytoplankton blooms.

1. Introduction

The Southern Ocean is the largest 'High Nitrate Low Chlorophyll' (HNLC) region of the global ocean (Buesseler et al., 2004), as a consequence of low iron (Fe) supply and subsequent reduced phytoplankton growth (Buesseler et al., 2004; Tsuda et al., 2009). Iron can be supplied to surface waters of the Southern Ocean by atmospheric dust inputs (Cassar et al., 2007; Gao et al., 2001), horizontal/vertical advective and diffusive mixing processes (de Jong et al., 2012), resuspension from shelf sediments (Kalnejais et al., 2010; Marsay et al., 2014), melting of icebergs and glaciers (Raiswell et al., 2008), and hydrothermal inputs (German et al., 2016). Despite the overall HNLC status of the Southern Ocean, regions in the wake of islands feature large seasonal phytoplankton blooms; the Fe sources to these blooms are however poorly constrained (de Jong et al., 2012; Planquette et al., 2007; Pollard et al., 2009).

Downstream of the island of South Georgia intense, long-lasting phytoplankton blooms have been observed which extend hundreds of kilometres, and require an enhanced Fe supply. The blooms peak in austral summer (Borrione et al., 2013), stretch over an area of ~ 750,000 km^2 (Atkinson et al., 2001; Korb et al., 2004), and are responsible for the largest dissolved inorganic carbon deficit reported within the Antarctic Circumpolar Current (ACC) (Jones et al., 2015; Jones et al., 2012). As a consequence of the Fe fertilisation, the waters in the vicinity of South Georgia support extensive phytoplankton blooms and a large biomass of zooplankton, fish, seabirds and marine mammals, some of which are exploited commercially (Atkinson et al., 2001; Murphy et al., 2007).

South Georgia forms part of the volcanically active Scotia Arc in the Atlantic sector of the Southern Ocean and is surrounded by a broad 30 to 100 km wide shelf with an average (albeit highly variable) depth of ca. 200 m (Fig. 1). The island is situated between the Antarctic Polar Front (PF) and the Southern ACC Front (SACCF), within the general northeast flow of the ACC (Meredith et al., 2005; Whitehouse et al., 2008). The ACC surface waters are enriched in nitrate, phosphate and silicic acid, but strongly depleted in most trace elements, notably Fe and manganese (Mn) (Browning et al., 2014). The large seasonal phytoplankton blooms downstream of South Georgia are thought to be

8

277 supplied with Fe from the island during the passage of ACC waters (Borrione et al., 2013; Nielsdóttir

278 et al., 2012).

279   In this study we provide the first comprehensive data set of dissolved and (labile) particulate

280 Fe, Mn, and Al in sediments, pore waters, and the water column overlaying the shelf and shelf edge

281 regions of South Georgia. We also include published data on the role of Antarctic krill in new Fe

282 supply and recycling in this region (Schmidt et al., 2011; Schmidt et al., 2016). We discuss

283 differences between the various analysed trace metal fractions and the supply routes of dissolved and

284 (labile) particulate Fe, such as sedimentary pore water efflux, supply of sediment derived particulate

285 Fe to the surface mixed layer, efflux of Fe from glacial melting and supply of Fe by faecal pellets of

286 Antarctic krill. Furthermore, we discuss the productivity of the bloom region to the north of South

287 Georgia in relation to the estimated Fe supply rates.

288

289 2. Methods

290 2.1 Cruises and Sampling

291   Samples were collected during three research cruises to South Georgia in 2011 (JR247,

292 JC055), and 2013 (JR274). While cruises JR247 and JR274 aimed to examine the pelagic shelf

293 ecosystem by collection of predominantly water samples (and zooplankton during JR247) on the

294 northern shelf, JC055 explored solely the composition of sediments on the southern shelf of South

295 Georgia. Cruise JR247 took place in January 2011 on RRS *James Clark Ross*, and 14 sites on the

296 northern shelf and shelf edge of South Georgia were visited (stations 1 – 21; Fig. 1). Suspended

297 particles were collected on acid cleaned polycarbonate filters (1 μm pore size; Whatman) using in-situ

298 Stand-Alone Pumping Systems (SAPS; Challenger Oceanic) attached to a Kevlar wire and deployed

299 at 20 m, 50 m and 150 m depth (Fig. 1, red dots). The filters were rinsed with deionized water (Milli-

300 Q; Millipore), stored at -20°C, and shipped frozen to the National Oceanography Centre Southampton

301 (NOCS).

302   Subsurface seawater samples were collected by trace metal clean samplers (Ocean Test

303   Equipment (OTE)) at 9 of the 14 SAPS locations (Fig. 1; black stars). Seawater samples were filtered

304   using cartridge filter (0.2 µm Sartobran P300; Sartorius) into acid cleaned 125 mL low-density

305   polyethylene (LDPE) bottles (Nalgene). Unfiltered samples were collected in 125 mL LDPE bottles

306   for analysis of total dissolvable (TD) trace metals. Surface waters from the South Georgia shelf were

307   collected using a tow fish deployed alongside the ship at 3 – 4 m depth. Samples were filtered in-line

308   using a cartridge filter (0.2 µm Sartobran P300; Sartorius) and dispensed in acid washed 125 mL

309   LDPE bottles. Unfiltered surface seawater samples were collected and dispensed in acid washed 125

310   mL LDPE bottles. All seawater samples were acidified on-board with ultra clean HNO_3 (15 M UpA

311   grade, Romil) to pH 1.7 (22 µmol H^+ L^{-1}). For a more detailed description of all sample-handling

312   procedures, please see Supplementary Text S1.

313   In January and February 2013, RRS *James Clark Ross* cruise JR274 revisited South Georgia

314   and collected surface seawater samples covering the shelf, shelf-edge, and open ocean areas around

315   the island. Dissolved and TD trace elements in surface seawater samples were collected using the tow

316   fish and treated similarly to samples from JR247. For a more detailed description of all sample-

317   handling procedures, please see Supplementary Text S1.

318   During the RRS *James Cook* cruise JC055 in February 2011, a megacorer (Bowers and

319   Connelly type) was used to collect surface sediment and pore water samples on the southern side of

320   South Georgia (there was no opportunity to sample the northern side of the island). Cores

321   representing the intact sediment – water interface were retrieved from three sites on the southern

322   shelf, at water depths of ca. 250 m (S1 – S3) (Fig. 1, blue hexagons). Pore waters were separated by

323   centrifugation under N_2 atmosphere and filtered using cellulose nitrate syringe filters (0.2 µm pore

324   size; Whatman (Homoky et al., 2012). Conjugate sediments were freeze dried on board and stored at

325   room temperature. A more detailed description of sediment and pore water sample-handling

326   procedures is provided in Supplementary Text S2.

Kommentar [SC2]: As suggested by reviewer1 we included the following sentence.

Kommentar [SC3]: We included now why sediment samples were sampled on the southern side of the shelf

327   Krill faecal pellets were obtained during on-board krill incubations performed during JR247.

328 Incubations were performed in darkness in the laminar flow cabinet at ambient surface layer

329 temperature. The krill were incubated in filtered seawater from the tow fish for up to ~3 h

330 immediately after capture, so that pellets obtained derived from material ingested in situ. These

331 incubations and their results are described in more detail in Schmidt et al. (2016).

332

2.2 Trace metal analysis in suspended particles and krill faecal pellets

334   The labile trace metal fraction of suspended particles (SAPS) and krill faecal pellets,

335 was remobilized using a 25% acetic acid solution (glacial SpA, Romil) following Planquette

336 et al. (2011). The labile trace metal fraction is hereafter referred to as the leachable

337 particulate trace metal fraction (LP). The remaining particles were digested on a hot plate

338 applying a mixture of aqua regia and hydrogen fluoride (Planquette et al., 2011). This

339 fraction will be referred to as the refractory particulate fraction (RP). The particulate trace

340 metal fraction (P) is the sum of leachable particulate (LP) and refractory particulate (RP). All

341 samples were analysed by collision cell inductively coupled plasma - mass spectrometry

342 (ICP-MS) (ThermoFisher Scientific, XSeriesII). For more detailed description of measured

343 certified reference material see Supplementary Text S1.

344

2.3 Trace metal analysis of seawater

346   The filtered and unfiltered seawater samples were stored for a period of 12 months prior to

347 analysis. Concentrations of dissolved and total dissolvable Fe, Mn, and Al in seawater were

348 determined by off-line pre-concentration and isotope dilution / standard addition ICP-MS

349 (ThermoFisher Scientific Element2 XR) according to Rapp et al. (2017). For a more detailed

350 description of the method and measured reference materials see Supplementary Text S1.

Kommentar [SC4]: We included, how faecal pellets were collected.

351

2.4 Trace metal analysis of pore waters and sediments

Sub-samples of the bulk, homogenized sediments were fully dissolved following an aqua regia and combined hydrofluoric/perchloric acid digestion method following Homoky et al. (2011). The acid digests and pore waters were analysed by ICP-optical emission spectrometry (OES) (Perkin Elmer Optima 4300DV). For a more detailed description of the method and measured reference materials see Supplementary Text S2.

358

3. Results & Discussion

3.1 Supply routes of suspended particulate Fe, Mn, and Al

3.1.1 Characterization of (the two) particulate trace metal fractions

Two different particulate fractions were obtained from samples collected during JR247; a particulate fraction from suspended particles collected using 1 μm pore size SAPS filters (P) and a leachable particulate fraction from unfiltered acidified seawater samples (LP_{Un}) collected at the same depth. LP_{Un} was calculated following Eq. (1):

$$LP_{Un} = \text{total dissolvable (TD; unfiltered)} - \text{dissolved (D; 0.2 μm filtered)} \qquad (1)$$

Because of the different sampling approaches (SAPS vs. OTE water samplers), filter sizes (>1 μm for SAPS vs. >0.2 μm for dissolved seawater) and digestion procedures (aqua regia + HF for SAPS particles vs. water sample storage at pH 1.7 [22 μmol H^+ L^{-1}]), concentrations of LP_{Un} and P differed, but showed similar distribution patterns in the water column (Fig. 2, Table 1 and 2). The concentrations of Fe, Mn and Al in the LP_{Un} fraction (LP_{Un}Fe, LP_{Un}Mn, LP_{Un}Al) were slightly lower than the particulate fraction from suspended particles (PFe, PMn, PAl). The LP_{Un} of unfiltered seawater samples corresponded to ~ 63 ± 4 % of the PFe, 83 ± 11% of the PAl and 100 ± 10% of the PMn fractions obtained by SAPS. The average LP_{Un} trace metal ratios (LP_{Un}Fe/ LP_{Un}Mn = 33.07 $\pm$

375 3.45 (1 σ) and $LP_{Un}Fe/ LP_{Un}Al = 0.65 \pm 0.10$ (n=69)), were about half of the elemental ratios of

376 suspended particles obtained by SAPS ($PFe/PMn = 68.0 \pm 0.6$ and $PFe/PAl = 1.251 \pm 0.042$ (n=42)

377 (Fig. 3; Table 1 and 2)).

378   The lower concentrations of Fe and Al and the reduced elemental ratios in the LP_{Un} compared

379 to the P fractions suggests that an unknown fraction of particulate Fe and Al in seawater was not

380 leached during the acidification procedure at pH 1.7 over 12 months. However, since P and LP_{Un}

381 displayed similar trends with depth (Fig. 2), LP_{Un} was used in sections 3.1.3 and 3.3 as an indicator

382 for the abundance of particulate trace metals at locations where particulate samples could not be

383 retrieved by SAPS, e.g. in surface waters collected by the tow fish and depths greater than 150 m.

384

385 3.1.2 Suspended particulate trace metals in the water column

386   Concentrations of PFe, PMn and PAl in the water column ranged from $0.87 - 267$ nmol L^{-1},

387 $0.01 - 3.85$ nmol L^{-1}, and $0.60 - 195$ nmol L^{-1}, respectively (Fig. 2, Table 2). Concentrations of

388 $LP_{Un}Fe$, $LP_{Un}Mn$ and $LP_{Un}Al$ ranged from $1 - 118$ nmol L^{-1}, $0.01 - 100$ nmol L^{-1}, and $1 - 141$ nmol L^{-1}

389 , respectively (Fig. 2, Table 1). Below the isopycnal density layer 27.05 kg m^{-3}, located at ~50 – 70

390 m depth, P and LP_{Un} increased with depth and showed a maximum near the seafloor of e.g. 207 nmol

391 L^{-1} for PFe and 112 nmol L^{-1} for $LP_{Un}Fe$ (#17, Table 2). Most sites on the shelf (bottom depth ≤ 260

392 m; #9/10, #13, #14, #17, and #21) showed seafloor maxima, in agreement with other shelf studies.

393 For example, Milne et al. (2017) reported concentrations of up to 140 nmol L^{-1} for PFe and 800 nmol

394 L^{-1} for PAl in bottom waters on the west African shelf, and Chase et al. (2005) showed bottom water

395 maxima of up to 400 nmol L^{-1} for $LP_{Un}Fe$ off the Oregon coast.

396   Strong linear relationships between elements were observed for suspended particles (SAPS)

397 obtained from above and below the 27.05 kg m^{-3} isopycnal, with elemental ratios of $PFe/PMn = 68.0$

398 ± 0.6 and $PFe/PAl = 1.25 \pm 0.04$ (n=42) (Fig. 3, Table 2). These elemental ratios were higher than

399 those reported for the earth's crust (Fe/Mn = 58, Fe/Al = 0.2, Fe/Ti (titanium) = 9.1 (Wedepohl,

400 1995)) and sediment samples collected to the south of the island (mean sediment surface layer of S1,

S2, S3; SFe/SMn = 51.5 ± 2.4, SFe/SAl = 0.34 ± 0.02 (Fig. 4, Table 3), and SFe/STi = 9.9 (not shown)), suggesting that the suspended particles were more enriched in Fe than lithogenic particles. We are aware that other trace metals, such as Ti, would be more appropriate than Mn to indicate the lithogenic origin of suspended particles. However, the element Ti was not monitored for dissolved, unfiltered seawater and particulate samples obtained by SAPS.

The Fe/Mn ratios among different phytoplankton species show strong variations but are typically much lower (Fe/Mn ~ 1.7 (Ho et al., 2003)), with also lower Fe concentrations than terrestrial/sediment particles (cellular concentration of phytoplankton ~ 0.7 mmol kg^{-1} (Ho et al., 2003); upper crust ~ 550 mmol kg^{-1} (Wedepohl, 1995)). A prevalence of biogenic particles in the suspended particle pool would be expected to result in reduced PFe/PMn ratios in our SAPS samples to values less than 51.5 as was observed in the sediments.

It is most likely that scavenging of DFe onto suspended lithogenic/sediment particles increased the Fe to Al (and Fe to Mn) ratio of suspended particles (PFe/PAl = 1.25; PFe/PMn = 68.0) compared to sediment particles (SFe/SAl = 0.34; SFe/SMn = 51.5). At seawater pH (~pH 8), dissolved Fe(III) is rapidly hydrolysed to soluble Fe(III)(OH)$_3$ (< 0.02 μm) which readily accumulates as nanometer sized colloids (0.02 – 0.2 μm) (Liu and Millero, 2002). It has been shown that both soluble and colloidal Fe are attracted by charged surfaces, a process that removes DFe and simultaneously increases the amount of particulate Fe in seawater over time (Schlosser et al., 2011).

A range of mechanisms delivers suspended particles to the surface waters. These transport mechanisms will be discussed in the following section.

3.1.3 Glacial outflow and zooplankton feeding activity

While most stations on the shelf showed bottom water maxima of particulate metals, at three sampling sites located on the shelf (#18) and shelf edge (#15/16 and #19/20), the particulate trace metal concentrations featured maxima in the top 100 m of the water column (Fig. 2 and 5). At site

426 #19/20, ca. 100 km away from the coast with a water depth of 1.741 m, the PFe concentration at 20 m

427 depth was 97 nmol L^{-1}, similar to $LP_{Un}Fe$ (Fig. 5). The elemental ratio PFe/PAl of these samples (e.g.

428 1.01 for site #19/20, 20 m depth) were close to the average ratio (PFe/PAl = 1.25), indicating that

429 lithogenic particles enriched with surface bound Fe dominated the suspended particulate pool in these

430 surface waters.

431   The surface water maxima of trace metals could have two supply routes: 1) lateral transport of

432 waters containing lithogenic particles from shallow island shelf sediments, and 2) transport of glacial

433 particles following melt processes. The reduced salinities (~33.3) recorded in surface waters in

434 Cumberland Bay and ~50 km offshore of South Georgia (~33.8) (Fig. 6(c) and S1) provide an

435 indication of glacial outflow, melting of icebergs and run-off of melt water streams. Enhanced

436 $LP_{Un}Fe$ concentrations of 2.2 μmol L^{-1} in low salinity surface waters inside Cumberland Bay, are

437 indicative of a meltwater source (LP_{Un} concentration used as only water samples from the tow fish

438 available). The $LP_{Un}Fe$ concentration decreased strongly with increasing distance from the coast, and

439 exhibited an abrupt reduction to 1 – 5 nmol Fe L^{-1} at the shelf edge ~ 100 km offshore. A similar

440 distribution pattern was observed for $LP_{Un}Mn$ (Fig. 6(d)) and $LP_{Un}Al$ (not shown), for cruises JR247

441 and JR274. Glacial melt has been reported as an important source of particulate material in the

442 vicinity of the Antarctic Peninsula (de Jong et al., 2012). For example, Gerringa et al. (2012)

443 documented elevated total dissolvable Fe concentration of up to 106 nmol L^{-1} near the Pine Island

444 Glacier in the Amundsen Sea, and Raiswell et al. (2008) estimated that per year 1.6 Gmol

445 nanoparticulate Fe, associated to terrigenous particles, are delivered to the Southern Ocean by melting

446 ice.

447   Locally elevated particulate metal concentrations in surface waters may also be related to

448 production of faecal pellets by swarms of Antarctic krill (Schmidt et al., 2016). High abundances of

449 Antarctic krill were estimated from acoustic backscattering observations (Fielding et al., 2014), and

450 large numbers of faecal pellets were observed on the SAPS filters during cruise JR247. The stomach

451 content of Antarctic krill contained up to 90% sediment particles by volume, an observation that was

452 attributed to filter feeding by these organisms on phytoplankton and seabed detritus, with incidental

15

453 ingestion of deep ocean sediments (Schmidt et al., 2011) and glacial flour (Schmidt et al., 2016).

454 Krill thus take up lithogenic particles and transfer these into the surface ocean through the egestion of

455 faecal pellets (Schmidt et al., 2016). The trace metal contents of krill faecal pellets collected during

456 on-board incubation experiments during JR247 ranged from 0.88 – 67.14 µg Fe mg^{-1} dry weight (n =

457 27) (Table 4) (Schmidt et al. 2016). The molar ratio PFe/PMn = 70.5 ± 8.21 of the faecal pellets was

458 similar to those for suspended particles in the water column (PFe/PMn = 68.0 ± 0.6; Table 1, 2 and 4),

459 indicating that Fe in krill faecal pellets was predominately associated with terrigenous material and/or

460 glacial flour particles, as also reported by Schmidt et al. (2016). In contrast, the molar ratio PFe/PAl

461 = 0.48 ± 0.07 of faecal pellets was lower than that of suspended particles, PFe/PAl = 1.25 ± 0.04, but

462 higher than that of sediments, PFe/PAl = 0.34 ± 0.02. The observed variability in the PFe/PAl ratio in

463 the various particle pools is therefore a consequence of different contributions of biogenic material to

464 the particulate reservoir and different amounts of Fe scavenged onto particle surfaces.

465

466 **3.2 Supply routes of dissolved Fe, Mn, and Al**

467 Concentrations of DFe, DMn, and DAl in the water column showed strong variations and

468 ranged from ~ 0.1 – 25.9 nmol L^{-1}, 0.3 – 19.6 nmol L^{-1} and 0.1 – 18.4 nmol L^{-1}, respectively (Fig. 2, 5

469 and 7), with highest values in the surface waters in Cumberland Bay, and lowest beyond the shelf

470 break (Fig. 6). Dissolved Fe concentrations from this study are in agreement with reported DFe near

471 the Antarctic Peninsula (0.6 – 14.6 nmol L^{-1} (de Jong et al., 2012)) and Crozet Islands (0.1 – 2.5 nmol

472 L^{-1} (Planquette et al., 2007)). Sources and sinks of dissolved trace metals, and their distribution in the

473 water column are discussed in the following sections.

474

475 3.2.1 Supply from sediment pore waters

476 Elevated pore water concentrations of Fe and Mn (Fe$_{PW}$ and Mn$_{PW}$) were observed in

477 sediments from the southern shelf sites at water depths of around 250 m, and ranged from 0.5 – 110

Kommentar [SC9]: For clarity we introduced the following sentences

478 μmol L^{-1} for Fe and 0.1 – 2 μmol L^{-1} for Mn (Fig. 7 and Table S2). The down-core distributions of

479 Fe$_{PW}$ and Mn$_{PW}$ were consistent with microbial dissimilatory Mn and Fe reduction during organic

480 matter oxidation (Canfield and Thamdrup, 2009), and thus concentrations were elevated at defined

481 depth horizons controlled by their redox potential (Eh) (Bonneville et al., 2009; Raiswell and

482 Canfield, 2012). The Fe$_{PW}$ and Mn$_{PW}$ concentrations near the sediment-seawater interface were used

483 to calculate fluxes of Fe and Mn to bottom waters following diffusion of reduced Fe and Mn species

484 across an oxygenated layer in surface sediments. These calculations were performed following

485 Boudreau and Scott (1978) and Homoky et al. (2012), and are described in detailed in the

486 Supplementary Text S3 and Table S1. We are aware that our calculated fluxes represent minimum

487 estimates of pore water efflux, which under natural conditions is supplemented by advection due to

488 bioirrigation, bioturbation, and bottom water currents (Homoky et al., 2016). In addition, sediment

489 cores were collected on the southern shelf, while seawater and particulate samples were collected on

490 the northern shelf side. The benthic Fe fluxes for the southern shelf maybe lower than those on the

491 northern shelf, as an elevated primary productivity and enhanced particle export on the northern side

492 will result in enhanced bacterial respiration, which reduces Eh and promotes the dissolution of Fe

493 oxides with subsequent release of Fe into bottom waters.

494   Notwithstanding the above issues, we calculated substantial benthic fluxes from sediment

495 pore waters to bottom waters on the southern shelf for Fe$_{PW}$ of <0.1 to 44.4 μmol m^{-2} d^{-1} and Mn$_{PW}$ of

496 0.6 to 4.1 μmol m^{-2} d^{-1}. The upper flux values for Fe are comparable to those reported for dysoxic and

497 river-dominated continental margins (3.5 – 55 μmol m^{-2} d^{-1} (Homoky et al., 2012)), seasonal maxima

498 of temperate and oxic shelf seas (23 – 31 μmol m^{-2} d^{-1} (Klar et al., 2017)), and shelf sediments off the

499 Antarctic Peninsula (1.3 – 15.5 μmol m^{-2} d^{-1} (de Jong et al., 2012)). The Mn fluxes were relatively low

500 for shelf environments, with for example fluxes of 70 – 4450 μmol m^{-2} d^{-1} reported for Baltic and

501 Black Sea sediments (Pakhomova et al., 2007)). The Fe pore water fluxes from the South Georgia

502 shelf sediments, which extend over an area of ca. 40,000 km^2, indicate that these may serve as an

503 important year-round source to overlying waters, totalling 4 to 1,728 kmol DFe d^{-1} and 25 to 164

504 kmol DMn d^{-1}.

Kommentar [SC10]: For clarity, we included the following sentences as suggested by reviewer1.

505   Benthic release of trace metal enriched pore waters shaped the distributions of dissolved trace

506   metals in bottom waters on the shelf. Concentrations of DFe, DMn, and DAl were enhanced at

507   isopycnals > 27.05 kg m^{-3} (e.g. DFe up to 7.70 nmol L^{-1} at site #21, Table 1) compared to surface

508   waters (e.g. DFe as low as 0.30 nmol L^{-1} at site #13, Table 1; Fig. 2 and 7). Trace metal enriched

509   bottom waters were also observed at sites #13, #14, #17 and #18 (Fig. 2). The molar DFe/DMn ratios

510   in oxygenated bottom waters varied between 1.1 – 3.5 and were thus similar to pore waters near the

511   sediment-seawater interface (0 – 1 cm depth, $Fe_{PW}/Mn_{PW} = 2.2 \pm 1.0$; Fig. 7). The similar trace metal

512   ratios suggest that Fe and Mn in enriched pore waters crossed the sediment-bottom water interface

513   and accumulated in shelf bottom waters.

514   To determine the vertical DFe fluxes from near bottom to surface waters we employed a

515   method outlined by de Jong et al. (2012), and calculated both the advective and diffusive flux terms,

516   which are not affected by the benthic Fe and Mn fluxes. We included the advective term in our

517   calculations, because it has been shown that internal waves that cross shallow topographies and wind

518   shear stress produces strong turbulence that facilitate Eckman upwelling (vertical advection) on the

519   shelf (Kurapov et al., 2010; Moore, 2000; Wolanski and Delesalle, 1995). Applying literature values

520   from the Southern Ocean for vertical diffusivity ($K_Z = 1$ x 10^{-4} m^2 s^{-1} (Charette et al., 2007)) and

521   advective velocity ($w = 1.1$ x 10^{-6} m s^{-1} (de Jong et al., 2012)), an average vertical DFe flux on the

522   shelf of 0.41 ± 0.26 µmol m^{-2} d^{-1} from subsurface waters into the surface mixed layer was estimated

523   (Supplementary Text S4). The surface mixed layer depth was determined by a density criteria (~0.03

524   kg m^{-3} (de Boyer Montégut et al., 2004)) and was located at ~50 m depth. About 38% of the DFe flux

525   was related to Ekman upwelling (advective term) and 62% to the diffusive flux. This vertical flux is at

526   the lower end of the calculated benthic flux from this study ($Fe_{PW} < 0.1$ to 44.4 µmol m^{-2} d^{-1}), and

527   agrees with values reported for other Southern Ocean shelf regions near the Antarctic Peninsula

528   (within 20 – 70 km from the coast: ~ 2.7 ± 3.4 µmol m^{-2} d^{-1} (de Jong et al., 2012)) and the Crozet

529   Islands (only diffusive flux of 0.06 µmol m^{-2} d^{-1} (Planquette et al., 2007)).

530

Kommentar [SC11]: For clarity we included the following sentence.

18

531   3.2.2 DFe supply from the leachable particulate fraction

532   The analytical protocol for the analysis of SAPS-collected particulate material allows separate

533   estimation of the refractory and leachable fractions of trace elements (RP and LP, respectively). The

534   RP fraction of the suspended matter is considered to include silicates and aged oxide minerals, while

535   the LP fraction represents predominantly oxyhydroxides, biogenic material and loosely bound surface

536   associated elements which are readily remobilized using leaching procedures (Berger et al., 2008).

537   Concentrations of LPFe, LPMn and LPAl in the water column showed strong variations,

538   ranging from a few picomoles to several nanomoles L^{-1} (Table 2). On average, LPFe and LPAl

539   concentrations at 150 m depth (~ 1.3 nmol LPFe L^{-1} and ~0.95 nmol LPAl L^{-1}) were significantly

540   higher than at 20 and 50 m, LPFe = 0.3 nmol L^{-1} (student t-test: t[0.95;28] = 1.725 [1.703];

541   t[confidence level; n-1]); LPAl = 0.43 nmol L^{-1} (student t-test: t[0.90;28] = 1.383 [1.313]). The

542   LPMn concentrations did not vary strongly and remained near constant throughout the top 150 m

543   (LPMn = 8.9 pmol L^{-1} {student t-test: [0.65;28] = 0.400 [0.390]}). The average contribution of LP to

544   the particulate pool, RP+LP, was low; 0.83 ± 1.13% for Fe, 2.55 ± 1.58% for Mn and 2.42 ± 1.32%

545   for Al (Table 2). A study conducted in the North Pacific near the Columbia River outflow, reported

546   considerably higher LP fractions (e.g. 6.6±3.0% of Fe, 78.7±14.0% of Mn, 6.3±2.0% of Al (Berger et

547   al., 2008)), which was attributed to enhanced biogenic particle levels in the low salinity waters of the

548   river (Berger et al., 2008). In contrast, results from our study showed that particulate trace metals

549   predominately had a refractory component (RP), indicating that Fe, Mn, and Al was mainly

550   incorporated in lithogenic material.

551   A weak linear relationship between RP and LP was observed for Fe (R^2 = 0.57, n = 41), Mn

552   (R^2 = 0.64, n = 41) and Al (R^2 = 0.63, n = 41) (Supplementary Fig. S2 and S3), indicating that the LP

553   fraction included mainly Fe, Mn and Al that was scavenged onto lithogenic particle surfaces and not

554   much LPFe was incorporated in biogenic particles. The scavenging of dissolved trace metals by

555   charged particle surfaces is established (Homoky et al., 2012; Koschinsky et al., 2003), but how well

556   Fe and other trace metals can be remobilized from marine particle surfaces and which process may

557 modify their availability over time is not yet well constrained (Achterberg et al., 2018; Fitzsimmons

558 and Boyle, 2014; Milne et al., 2017).

559 For instance, scavenged Fe is reported to exchange with DFe in the water column of the

560 tropical and high latitude North Atlantic (Achterberg et al., 2018; Fitzsimmons and Boyle, 2014;

561 Milne et al., 2017). In addition, recent work has concluded that zooplankton grazing and the

562 production of faecal pellets remobilizes DFe from lithogenic and biogenic particles (Giering et al.,

563 2012; Schmidt et al., 2016). In contrast, freshly produced inorganic Fe(III) oxyhydroxide (FeOOH *

564 nH_2O) precipitates in seawater are subject to chemical and structural conversions that lead to less

565 soluble Fe with time (Yoshida et al., 2006).

566

567 3.2.3 DFe supply from Antarctic krill

568 Elevated dissolved trace metal concentrations in the top 200 m of the water column coincided

569 with elevated particulate trace metal concentrations at sites #11/12, #15/16, #18, and #19/20 (Fig. 2, 5,

570 and 7). The SAPS filters from these stations contained a high load of krill faecal pellets. To elucidate

571 the relationship between dissolved trace metal concentrations and the local abundance of Antarctic

572 krill and their faecal pellets, krill were caught and incubated on-board the vessel as described in

573 Schmidt et al. (2016).

574 Antarctic krill excretion rates of DFe were variable, relating positively to the extent of recent

575 ingestion of diatoms. However, on average krill released ~2.0 ± 1.9 nmol DFe individual^{-1} d^{-1}

576 (Schmidt et al., 2016). By applying a mean krill abundance of 465 ± 588 individuals m^{-2}, estimated

577 from acoustic backscattering measurements (Fielding et al., 2014), krill excreted 1.1 ± 2.2 μmol DFe

578 m^{-2} d^{-1} into the top 300 m of the water column (Schmidt et al., 2016). In addition, krill produced ca.

579 1.8 ± 1.6 mg of faecal pellets per individual per day. Particle leaches performed on those faecal pellet

580 samples with 25% acetic acid showed that on average 2.5 ± 2.1% of the total Fe in these pellets could

581 be remobilised (Table 4), which would equate to a production of 14 ± 24 nmol LPFe ind^{-1} d^{-1}. By

Kommentar [SC12]: We modified the paragraph

582 multiplying the mean LPFe by the ambient krill density used above, we calculate a LPFe flux of 6.5 ±

583 8.2 μmol m^{-2} d^{-1} from the faecal pellets to the water column.

584   Since krill are mobile animals, questions remain over where the major part of the LPFe flux

585 occurs, and what the fate of this Fe source is. Highest krill abundances were recorded generally (but

586 not exclusively) in the top 100 m layer (Fielding et al., 2014), and hence a large proportion of this

587 LPFe flux from krill is likely to occur in the upper waters. Notwithstanding our current uncertainties

588 over the depths of origin and fate, the LPFe flux from krill faecal pellets and the release of DFe were

589 on average an order of magnitude higher than estimated vertical diffusive and advective DFe fluxes,

590 with other grazers, such as copepods and salps, adding to the recycled flux estimates. This illustrates

591 the importance of zooplankton-mediated-Fe-cycling, in agreement with previous studies (Hutchins

592 and Bruland, 1994; Sato et al., 2007).

593   The experimental set-up did not allow us to establish the origin of the Fe released by krill,

594 being both "recycled" Fe from biogenic material and "new" Fe from lithogenic material. However,

595 Schmidt et al. (2016) concluded that zooplankton gut passage mobilizes lithogenic Fe, and showed

596 that there are strong spatial patterns in the organic and lithogenic make-up of faecal pellets. This

597 included an exponential decline in the quantity of lithogenic particles in krill stomachs with distance

598 from sources of glacial flour on the northern South Georgia coast. For instance, the lithogenic content

599 at one site on the shelf contributed ~90% of stomach content volume suggesting that a large quantity

600 of the accessible Fe was remobilized from those inorganic particles.

601

3.3 Off-shore transport of trace metal enriched water masses

603   Along a W – E transect (Fig. 1; #14 via # 13 to #11/12), lateral water mass transport carried

604 suspended particles offshore. Because of the small size of the SAPS particulate data set (two data

605 points), we considered the LP$_{Un}$ fraction for this transect (Fig. 1). Indeed, elevated concentrations of

606 the P and LP$_{Un}$ metal fractions were observed in subsurface waters that had been in recent contact

607 with the shelf. These metal-enriched waters, detected at the eastern shelf edge site #11/12 between

Kommentar [SC13]: We included the following paragraph to distinguish between new and recycled Fe, as suggested by reviewer2.

Kommentar [SC14]: We modified the paragraph as suggested by reviewer1.

608 200 and 400 m water depth (Fig. 1 and 4), exhibited similar temperature and salinity signatures to

609 shelf bottom waters. Furthermore, the elemental ratios of the LP_{Un} fraction in these waters were

610 similar to the particles in the surface sediments (S1, S2, and S3) and the resuspended particles in the

611 bottom boundary layer (#13 and #14) on the shallow shelf (Fig. 4). A similar distribution was also

612 found for the P fractions, but limited to site #13 and #14, as SAPS were not deployed below 150 m at

613 the shelf edge site #11/12.

614   The LP_{Un}Fe concentration decreased with distance from the island to offshore: from site #14

615 at 200 m depth (LP_{Un}Fe = 82.26 nmol L^{-1}; water depth = 255 m) to site #13 at 100 m depth (LP_{Un}Fe =

616 34.06 nmol L^{-1}; water depth = 130 m) to site #11/12 between 200 and 400 m depth (LP_{Un}Fe ~ 10.18

617 nmol L^{-1}; water depth = 750 m) (Fig.4 and Table 1). A similar decrease was observed for the SAPS

618 Fe data: from site #14 at 150 m depth (PFe = 31.12 nmol L^{-1}) to site #13 at 100 m depth (PFe = 10.23

619 nmol L^{-1}). The decrease of PFe and LP_{Un}Fe with increasing distance to the coast is in agreement with

620 previous observations for the Western Subarctic Pacific (Lam and Bishop, 2008), which reported

621 elevated LPFe concentrations in the range of 0.6 to 3.8 nmol L^{-1} in subsurface waters between 100

622 and 200 m depth along the Kamchatka shelf and related this observation to offshore water mass

623 transport. However, we assume that particles in the deep particulate Fe maximum are not transported

624 over very large distances, due to their tendency to sink, and thus do not significantly contribute to the

625 offshore Fe supply (section 3.4).

626   Consistent with the observed P and LP_{Un} distributions, elevated dissolved metal

627 concentrations at depths between 200 and 400 m at site #11/12 indicated that trace metal enriched

628 shelf bottom waters were transported offshore (Fig. 7). However, dissolved trace metal concentrations

629 were more variable than P and LP_{Un}, and in case for DMn were highest at depths at shelf edge site

630 #11/12. Notwithstanding the above issue, for horizontal flux calculations we used the entire DFe data

631 set for water depths between 100 and 400 m. Average DFe concentrations in this depth range were

632 highly variable and did not follow an exponential or power law function with distance from the coast

633 (Supplementary Fig. S4), which is necessary to determine scale length and horizontal diffusivity (K_h)

634 (de Jong et al., 2012). As a result, horizontal flux calculations from the data could not be executed.

Kommentar [SC15]: We removed the exponential equations and rewrote the sentences.

Kommentar [SC16]: We included why particulate trace metals are not included in section 3.4

Kommentar [SC17]: As requested by reviewer 1 we included the following sentence.

22

635 The distribution of dissolved trace metals in surface waters indicated that there was a limited

636 transfer of DFe beyond the shelf break into the bloom region. Surface samples showed that DFe

637 concentrations were strongly enriched in surface waters on the shelf (0.3 – 25.9 nmol L^{-1}, Fig. 6(b)),

638 while DFe concentrations beyond the shelf break decreased abruptly to concentrations < 0.2 nmol L^{-1}

639 (Fig. 6(b)). This indicates that DFe was quickly removed from ACC surface waters following passage

640 of the island. However, previous studies in the region suggest DFe transfer beyond the shelf break of

641 South Georgia (Borrione et al., 2013; Nielsdóttir et al., 2012). Nielsdóttir et al. (2012) reported

642 surface waters downstream the island shelf with up to 2 nmol DFe L^{-1}, with seasonal variations and

643 highest concentrations during austral summer in January/February 2008. Dissolved Fe data from

644 JR247 (2011) and JR274 (2012) were also obtained during the summer season, but indicated rapid

645 reduction in concentrations through mixing with DFe depleted ACC water, biological uptake and/or

646 particle scavenging.

647

648 **3.4 Iron budget in the bloom region**

649 Large seasonal phytoplankton blooms downstream of South Georgia recorded by earth

650 observing satellites are initiated by Fe supplied by the South Georgia island/shelf system during the

651 passage of ACC waters (Fig. 1) (Borrione et al., 2013; Nielsdóttir et al., 2012). Based on our study,

652 the main DFe sources during this passage of the ACC were benthic release and vertical mixing,

653 release of DFe from krill and krill faecal pellets, and supply of particles from run-off and glacial

654 meltwater. In the following sections we will discuss the strength of each DFe source in the bloom

655 region ca. 1,250 km downstream of the island and estimate how much DFe is required to stimulate the

656 elevated primary productivity in that region. Because of the lack of observational data for the region,

657 this part of the study combines literature values from different Southern Ocean studies. This approach

658 contains large uncertainties that are discussed in detail in Section 3.4.6 Budget uncertainties.

659

660 3.4.1 Phytoplankton Fe requirements in the phytoplankton bloom region

Kommentar [SC18]: To show that the DFe budget remains uncertain we included the following sentence.

661   The surface ocean in the vicinity of South Georgia during the austral summer features

662 strongly elevated biomass production (Gilpin et al., 2002) and represents the largest known CO_2 sink

663 in the ACC (12.9 mmol C m^{-2} d^{-1} (Jones et al., 2012)). The Fe requirements of the phytoplankton

664 community in austral summer within the bloom that reaches more than thousand kilometres

665 downstream the island were determined by combining satellite-depth integrated net primary

666 production data derived from a phytoplankton pigment adsorption (α_{ph})-based model (62 ± 21 mmol C

667 m^{-2} d^{-1} (Ma et al., 2014)) over the period of 2003-2010 with an average intracellular Fe:C ratio

668 obtained from five Southern Ocean diatom species (5.23 ± 2.84 µmol Fe mol^{-1} C (Strzepek et al.,

669 2011)). This approach yielded an approximate Fe requirement of 0.33 ± 0.11 µmol DFe m^{-2} d^{-1} for

670 the phytoplankton community (Fig. 8). For a more detailed description of the applied values and

671 calculations see Supplementary Text S4.

672

673 3.4.2 Horizontal and vertical mixing

674   De Jong et al. (2012) reported that horizontal and vertical advective, diffusive (diapycnal) and

675 deep winter mixing downstream (1,250 – 1,570 km) of the Antarctic Peninsula (between 51°S and

676 59°S) supplied DFe to the surface waters in quantities that exceeded the DFe requirement of primary

677 producers during austral summer (0.13 ± 0.04 µmol DFe m^{-2} d^{-1}). In their study region, de Jong et al.

678 (2012) determined that ~ 0.30 ± 0.22 µmol DFe m^{-2} d^{-1} were supplied by horizontal and vertical

679 fluxes, of which 91% of the vertical flux were attributed to Ekman upwelling (advective term), and

680 43% of the entire DFe flux was supplied by deep winter mixing. Tagliabue et al. (2014) reported

681 similar model estimates for the region that is located south of the SACCF and characterized by strong

682 Ekman upwelling and winter entrainment.

683   For the bloom region downstream of South Georgia north of the SACCF, model calculations

684 by Tagliabue et al. (2014) indicated that less than 0.0003 µmol DFe m^{-2} d^{-1} were supplied by

685 diapycnal mixing, and ~ -0.0027 µmol DFe m^{-2} d^{-1} were removed by Ekman down-welling. For the

686 vertical flux component, this yields an overall loss of DFe of ~ -0.002 µmol DFe m^{-2} d^{-1} (0.0003 + (-

687 0.0027)) in the bloom region north of South Georgia (Fig. 8).

688 Because the sampling in our study was not suitable for calculations of the horizontal flux, we

689 applied the horizontal flux estimates from de Jong et al. (2012) for our own Fe budget. For a region

690 ca. 1,250 km downstream of a source, calculations according to de Jong et al. (2012) sugest that ca.

691 0.11 ± 0.03 µmol DFe m^{-2} d^{-1} are supplied to the bloom region by horizontal advection and diffusion

692 (Fig. 8).

693

694 3.4.3 Deep winter mixing

695 The entrainment of new DFe during winter represents an important Fe source to surface

696 waters in the Southern Ocean (de Jong et al., 2012; Tagliabue et al., 2014). Elevated DFe

697 concentrations in subsurface waters support primary production in the austral spring following

698 entrainment by deep winter mixing. Model estimates showed that DFe supplied by winter mixing,

699 together with diapycnal mixing, matches the Fe requirements at most low productivity sites in the

700 Southern Ocean. However, deep winter mixing at the highly productive sites north of South Georgia

701 supplies only ~ 0.011 µmol m^{-2} d^{-1} (Tagliabue et al., 2014) (Fig. 8). Later in the season primary

702 productivity in surface waters is considered to rely strongly on Fe derived from recycling of biogenic

703 material (Boyd et al., 2015).

704

705 3.4.4 Dust deposition

706 Dissolved Fe supplied by the deposition of aeolian dust is considered to be an important

707 source to the Southern Ocean (Conway et al., 2015; Gabric et al., 2010; Gassó and Stein, 2007).

708 Aeolian flux model estimates, supplied by Borrione et al. (2013) using a regional South Georgia

709 model, suggested that up to 8 µmol Fe m^{-2} d^{-1} are delivered to the bloom regions downstream of South

710 Georgia by dry and wet deposition. However, reliable dry and wet deposition estimates for the

711　Southern Ocean are limited. Data from the South Atlantic along 40°S, ~ 1.000 km north of South

712　Georgia, showed that rather low levels of DFe (~ 0.002 μmol m^{-2} d^{-1}) are supplied by dry deposition

713　(Chance et al., 2015). In addition, ~ 1.0 ± 1.2 μmol DFe m^{-2} d^{-1} are delivered sporadically to the 40°S

714　area by wet deposition (Chance et al., 2015). However, even when assuming that similar wet

715　deposition fluxes occur north of South Georgia, fertilization with DFe is temporally and spatially

716　limited. Furthermore, it is very unlikely that such sporadic events could cause long-lasting and far

717　extending phytoplankton blooms strictly constrained between the PF and the SACCF.

718

719　3.4.5 Luxury Fe uptake on the shelf

720　　　　Our conservative estimate of DFe supply to the bloom region by vertical/horizontal mixing,

721　deep winter entrainment and dust deposition (< 0.12 μmol Fe m^{-2} d^{-1}) covers only ~30% of the

722　estimated phytoplankton requirements (~ 0.33 μmol Fe m^{-2} d^{-1}) (Fig. 8). We hypothesize that the

723　missing supply of ~ 0.21 μmol DFe m^{-2} d^{-1} is supplied to the bloom region through the off-shore

724　advection of phytoplankton cells that are enriched in labile Fe. It has been demonstrated that Fe-rich

725　biogenic particles can be created by luxury iron uptake of diatoms (Iwade et al., 2006; Marchetti et al.,

726　2009). Using bottle incubation experiments, Iwade et al. (2006) showed that under Fe replete

727　conditions the coastal diatom *Chaetoceros sociale* stores more intracellular Fe than needed for the

728　production of essential enzymes and proteins. We therefore hypothesize that phytoplankton cells that

729　grew under excess nutrient supply on the South Georgia shelf stored more Fe than needed for their

730　metabolic processes. Due to subsequent cycles of grazing, lysis or bacterial decomposition, this iron

731　can be remobilised in surface waters and made available for renewed phytoplankton uptake.

732　　　　High Fe recycling efficiencies, described by the f*e* ratio (Boyd et al., 2005), are required to

733　maintain the cycle of remineralisation and uptake in the euphotic zone. This counteracts the loss of

734　particulate Fe by vertical export. Boyd et al. (2015) reported the highest recycling efficiencies of ~

735　90% for subantarctic, DFe-deplete waters such as downstream of South Georgia. Further, these

736　workers showed that the degree of recycling is controlled by the abundance of prokaryotes with a high

Kommentar [SC19]: We changed to "hypothesize" as suggested by reviewer1.

737 Fe quota, such as cyanobacteria, and particularly by grazing zooplankton. The waters off South

738 Georgia feature among the highest biomasses worldwide of metazoan grazers (Atkinson et al., 2001).

739 These large grazers, chiefly copepods and Antarctic krill, are able to efficiently ingest large diatoms

740 including species that are known to store luxury iron (Atkinson, 1994; Hamm et al., 2003), thereby

741 disintegrating cell membranes and releasing trace metals.

742 In recent years it has become apparent that the recycling of biogenic particles in the euphotic

743 zone is a critical mechanism that maintains primary production, especially when the dissolved nutrient

744 pools become exhausted (Boyd et al., 2015; Tagliabue et al., 2014). However, uncertainties remain

745 over the degree to which Fe is lost during each cycle of uptake and remineralisation. Thus more

746 research is needed, especially field work that encompasses the community structures (bacteria,

747 phytoplankton, zooplankton, and higher predators (Ratnarajah et al., 2017; Wing et al., 2014)), the

748 degree of recycling for macro- and micro-nutrients in the euphotic zone, and loss of Fe through

749 vertical export.

750 An alternative explanation to our suggestion that recycling of luxury iron enriched biota

751 contributes to the downstream bloom is that iron is adsorbed directly onto particles that are advected

752 directly offshore. For example freshly precipitated Fe(III) oxyhydroxides (FeOOH * nH$_2$O) may be

753 adsorbed onto biogenic and non-biogenic material. Iron freshly absorbed onto biogenic and non-

754 biogenic material can be released and incorporated by phytoplankton and bacteria. However, the

755 bioavailability of adsorbed and inorganic Fe changes over time. Both Wells et al. (1991) and Chen

756 and Wang (2001) demonstrated that the bioavailability of freshly precipitated FeOOH and Fe

757 adsorbed onto colloids/inorganic particles decreases over time. This is primarily due to the

758 dehydration of the loosely packed structure that is subsequently transferred into amorphous FeOOH in

759 the mineral structure Goethite. Because of this we suggest that the majority of Fe from inorganic

760 FeOOH or Fe adsorbed onto particles must be released and utilized in an early stage of the voyage,

761 mainly on the shelf or shortly after the shelf break.

762

Kommentar [SC20]: As requested by reviewer 2, we included alternative explanations.

3.4.6 Budget uncertainties

Estimates for Fe budgets are challenging and often contain large uncertainties. This is primarily due to the lack of site- and time-specific flux data. Moreover, the mean annual estimates, necessary for reliable supply calculations, reach a high level of accuracy only after the same region has been monitored multiple times to cover seasonal and annual anomalies. In the following, we will discuss the uncertainty of the different Fe fluxes in the blooming region north of South Georgia.

We identified three main processes that account together for ~98% of the total Fe flux in the blooming region, and thus contribute largest uncertainties; the horizontal flux, dry/wet deposition, and winter entrainment. Horizontal flux estimates of this study rely on literature values that were collected offshore the Antarctic Peninsula. In contrast, South Georgia is an island with a confined shelf region and thus horizontal DFe fluxes may differ greatly. Furthermore, we showed that dry deposition dust fluxes are generally low, but showed in addition that the Fe flux can be supplemented strongly by sporadic wet deposition events ($\sim 1.0 \pm 1.2$ μmol DFe m^{-2} d^{-1}) (Chance et al., 2015). Atmospheric fluxes are variable, illustrated by the large standard deviation of the wet deposition Fe fluxes obtained at 40°S. Furthermore, to determine the magnitude of the seasonal DFe winter entrainment reliable estimates of the winter mixing layer depth (WMLD) and the ferrocline are required. Even though the WMLD can be estimated very precisely using Argo float data, the depth of ferrocline in the manuscript of Tagliabue et al. (2014) is based on 140 unique observations distributed over the entire Southern Ocean. Due to this regional anomalies are not captured. In addition to the DFe fluxes in the blooming region, we also assume that the biological Fe demand estimated for the phytoplankton community contributes a large error. The biological Fe requirements were determined using satellite derived net primary production data and an average intracellular Fe:C ratio derived from 5 different diatom species native to the Southern Ocean. Both parameters are not well constrained and because of the lack of observational data we applied the lowest intracellular Fe:C ratio available in the literature (Strzepek et al., 2011). However, we found that even small changes of the both parameters change the estimated Fe availability in the bloom region strongly. Nevertheless, flux estimates even with large uncertainties can help us understand the degree of the nutrient supply vs. consumption by organisms

28

790 and help to pinpoint the limitation of the estimates made. To ultimately reduce the level of uncertainty

791 and to improve our biogeochemical models more observational data from the bloom region north of

792 South Georgia is required.

793

794 **4. Conclusions**

795 Shelf sediment-derived Fe and Fe released from Antarctic krill significantly contribute to the

796 DFe distribution in the shelf waters around South Georgia. Nevertheless, DFe enriched in shelf waters

797 are not effectively advected to the phytoplankton bloom region downstream of the island. Together

798 with other Fe supplies, such as aeolian dust, deep winter mixing and diapycnal mixing, the horizontal

799 advection contributes only ~30% to the Fe requirements of a phytoplankton bloom downstream of

800 South Georgia. We therefore hypothesize that the majority of the Fe is derived from remineralisation

801 of Fe enriched phytoplankton cells and biogenic particles that are transported with the water masses

802 into the bloom region.

Kommentar [SC22]: As requested by reviewer1 we hypothesize now that DFe was in addition transported as biological labile particulate Fe

803 While we highlight the importance of grazers and the cycling of various particulate Fe phases

804 in the Fe-fertilisation of the South Georgia bloom, more work is needed to clarify the transport

805 mechanisms of dissolved and particulate Fe.

Kommentar [SC23]: We removed some irrelevant sentences.

806

807 **Author contribution**

808 CS, KS, EPA, SF, and AAt designed the experiments for JC247. CS, MDP and AAt performed the

809 sampling and krill incubation experiments during JC247. CS and MC analysed the trace metal

810 samples at NOCS. EPA sampled the seawater during JC274. Samples from JC274 were analysed by

811 CS and MC. AAq, WBH and RM designed the experiments for JR55 and AAq analysed the samples.

812 CS prepared the manuscript with contributions from all co-authors.

813

814 **Acknowledgements**

820 **References**

821 Achterberg, E. P., Steigenberger, S., Marsay, C. M., LeMoigne, F. A. C., Painter, S. C.,

822 Baker, A. R., Connelly, D. P., Moore, C. M., Tagliabue, A., and Tanhua, T.: Iron

823 Biogeochemistry in the High Latitude North Atlantic Ocean, Scientific Reports, 8, 1283,

824 2018.

825 Atkinson, A.: Diets and feeding selectivity among the epipelagic copepod community near

826 South Georgia in summer, Polar Biol., 14, 551-560, 1994.

827 Atkinson, A., Whitehouse, M. J., Priddle, J., Cripps, G. C., Ward, P., and Brandon, M. A.:

828 South Georgia, Antarctica: a productive, cold water, pelagic ecosystem, Mar. Ecol.-Prog.

829 Ser., 216, 279-308, 2001.

830 Berger, C. J. M., Lippiatt, S. M., Lawrence, M. G., and Bruland, K. W.: Application of a

831 chemical leach technique for estimating labile particulate aluminum, iron, and manganese in

832 the Columbia River plume and coastal waters off Oregon and Washington, J. Geophys. Res.,

833 113, 1-16, 2008.

834 Bonneville, S., Behrends, T., and Van Cappellen, P.: Solubility and dissimilatory reduction

835 kinetics of iron(III) oxyhydroxides: A linear free energy relationship, Geochim. Cosmochim.

836 Act., 73, 5273-5282, 2009.

837 Borrione, I., Aumont, O., Nielsdottir, M. C., and Schlitzer, R.: Sedimentary and atmospheric

838 sources of iron around South Georgia, Southern Ocean: a modelling perspective,

839 Biogeosciences Discuss., 10, 10811-10858, 2013.

840 Boudreau, B. P. and Scott, M. R.: A model for the diffusion-controlled growth of deep-sea

841 manganese nodules, Americ. J. Sc., 278, 903-929, 1978.

842 Boyd, P. W., Law, C. S., Hutchins, D. A., Abraham, E. R., Croot, P. L., Ellwood, M., Frew,

843 R. D., Hadfield, M., Hall, J., Handy, S., Hare, C., Higgins, J., Hill, P., Hunter, K. A.,

844 LeBlanc, K., Maldonado, M. T., McKay, R. M., Mioni, C., Oliver, M., Pickmere, S.,

845   Pinkerton, M., Safi, K., Sander, S., Sanudo-Wilhelmy, S. A., Smith, M., Strzepek, R., Tovar-

846   Sanchez, A., and Wilhelm, S. W.: FeCycle: Attempting an iron biogeochemical budget from

847   a mesoscale SF6 tracer experiment in unperturbed low iron waters, Global Biogeochem.

848   Cycles, 19, 1-13, 2005.

849   Boyd, P. W., Strzepek, R. F., Ellwood, M. J., Hutchins, D. A., Nodder, S. D., Twining, B. S.,

850   and Wilhelm, S. W.: Why are biotic iron pools uniform across high- and low-iron pelagic

851   ecosystems?, Global Biogeochem. Cycles, 29, 1028-1043, 2015.

852   Browning, T. J., Bouman, H. A., Henderson, G. M., Mather, T. A., Pyle, D. M., Schlosser,

853   C., Woodward, E. M. S., and Moore, C. M.: Strong responses of Southern Ocean

854   phytoplankton communities to volcanic ash, Geophys. Res. Lett., 41, 1-7, 2014.

855   Buesseler, K. O., Andrews, J. E., Pike, S. M., and Charette, M. A.: The Effects of Iron

856   Fertilization on Carbon Sequestration in the Southern Ocean, Science, 304, 414-417, 2004.

857   Canfield, D. E. and Thamdrup, B.: Towards a consistent classification scheme for

858   geochemical environments, or, why we wish the term 'suboxic' would go away, Geobiol., 7,

859   385-392, 2009.

860   Cassar, N., Bender, M. L., Barnett, B. A., Fan, S., Moxim, W. J., Levy II, H., and Tilbrook,

861   B.: The Southern Ocean Biological Response to Aelian Iron Input, Science, 317, 1067-1070,

862   2007.

863   Chance, R., Jickells, T. D., and Baker, A. R.: Atmospheric trace metal concentrations,

864   solubility and deposition fluxes in remote marine air over the south-east Atlantic, Mar.

865   Chem., 177, 45-55, 2015.

866   Charette, M. A., Gonneea, M. E., Morris, P., Statham, P., Fones, G., Planquette, H., Salter, I.,

867   and Garabato, A. N.: Radium isotopes as tracers of iron sources fueling a Southern Ocean

868   phytoplankton bloom, Deep-Sea Res. II, 54, 1989-1998, 2007.

869 Chase, Z., Hales, B., Cowles, T., Schwartz, R., and van Geen, A.: Distribution and variability

870 of iron input to Oregon coastal waters during the upwelling season, J. Geophys. Res., 110, 1-

871 14, 2005.

872 Chen, M. and Wang, W.-X.: Bioavailability of natural colloid-bound iron to marine plankton:

873 Influences of colloidal size and aging, Limnol. Oceanogr., 46, 1956-1967, 2001.

874 Conway, T. M., Wolff, E. W., Rothlisberger, R., Mulvaney, R., and Elderfield, H. E.:

875 Constraints on soluble aerosol iron flux to the Southern Ocean at the Last Glacial Maximum,

876 Nat. Commun., 6, 1-9, 2015.

877 de Boyer Montégut, C., Madec, G., Fischer, A. S., Lazar, A., and Iudicone, D.: Mixed layer

878 depth over the global ocean: An examination of profile data and a profile-based climatology,

879 J. Geophys. Res., 109, 1-20, 2004.

880 de Jong, J., Schoemann, V., Lannuzel, D., Croot, P., de Baar, H. J. W., and Tison, J. L.:

881 Natural iron fertilization of the Atlantic sector of the Southern Ocean by continental shelf

882 sources of the Antarctic Peninsula, J. Geophys. Res., 117, 1-25, 2012.

883 Fielding, S., Watkins, J. L., Trathan, P. N., Enderlein, P., Waluda, C. M., Stowasser, G.,

884 Tarling, G. A., and Murphy, E. J.: Interannual variability in Antarctic krill (Euphausia

885 superba) density at South Georgia, Southern Ocean: 1997–2013, ICES J. Mar. Sci., 2014. 1-

886 11, 2014.

887 Fitzsimmons, J. N. and Boyle, E. A.: Both soluble and colloidal iron phases control dissolved

888 iron variability in the tropical North Atlantic Ocean, Geochim. Cosmochim. Act., 125, 539-

889 550, 2014.

890 Gabric, A. J., Cropp, R. A., McTainsh, G. H., Johnston, B. M., Butler, H., Tilbrook, B., and

891 Keywood, M.: Australian dust storms in 2002 and 2003 and their impact on Southern Ocean

892 biogeochemistry, Global Biogeochem. Cycles, 24, 1-17, 2010.

893   Gao, Y., Kaufman, Y. J., Tanré, D., Kolber, D., and Falkowski, P. G.: Seasonal distributions

894   of aeolian iron fluxes to the global ocean, Geophys. Res. Lett., 28, 29-32, 2001.

895   Gassó, S. and Stein, A. F.: Does dust from Patagonia reach the sub-Antarctic Atlantic

896   Ocean?, Geophys. Res. Lett., 34, 1-5, 2007.

897   German, C. R., Casciotti, K. A., Dutay, J.-C., Heimbürger, L. E., Jenkins, W. J., Measures, C.

898   I., Mills, R. A., Obata, H., Schlitzer, R., Tagliabue, A., Turner, D. R., and Whitby, H.:

899   Hydrothermal impacts on trace element and isotope ocean biogeochemistry, Philos Trans A

900   Math Phys Eng Sci, 374, 1-19, 2016.

901   Gerringa, L. J. A., Alderkamp, A.-C., Laan, P., Thuróczy, C.-E., De Baar, H. J. W., Mills, M.

902   M., van Dijken, G. L., van Haren, H., and Arrigo, K. R.: Iron from melting glaciers fuels the

903   phytoplankton blooms in Amundsen Sea (Southern Ocean): Iron biogeochemistry, Deep-Sea

904   Res. II, 71-76, 16-31, 2012.

905   Giering, S. L. C., Steigenberger, S., Achterberg, E. P., Sanders, R., and Mayor, D. J.:

906   Elevated iron to nitrogen recycling by mesozooplankton in the Northeast Atlantic Ocean,

907   Geophys. Res. Lett., 39, L12608, 2012.

908   Gilpin, L. C., Priddle, J., Whitehouse, M. J., Savidge, G., and Atkinson, A.: Primary

909   production and carbon uptake dynamics in the vicinity of South Georgia-balancing carbon

910   fixation and removal, Mar. Ecol. Prog. Ser., 242, 51-62, 2002.

911   Hamm, C. E., Merkel, R., Springer, O., Jurkojc, P., Maier, C., Prechtel, K., and Smetacek, V.:

912   Architecture and material properties of diatom shells provide effective mechanical protection,

913   Nature, 421, 841-843, 2003.

914   Ho, T.-Y., Quigg, A., Finkel, Z. V., Milligan, A. J., Wyman, K., Falkowski, P. G., and Morel,

915   F. M. M.: The elemental composition of some marine phytoplankton, J. Phycol., 39, 1145-

916   1159, 2003.

917 Homoky, W. B., Hembury, D. J., Hepburn, L. E., Mills, R. A., Statham, P. J., Fones, G. R.,

918 and Palmer, M. R.: Iron and manganese diagenesis in deep sea volcanogenic sediments and

919 the origins of pore water colloids, Geochim. Cosmochim. Act., 75, 5032-5048, 2011.

920 Homoky, W. B., Severmann, S., McManus, J., Berelson, W. M., Riedel, T. E., Statham, P. J.,

921 and Mills, R. A.: Dissolved oxygen and suspended particles regulate the benthic flux of iron

922 from continental margins, Mar. Chem., 134–135, 59-70, 2012.

923 Homoky, W. B., Weber, T., Berelson, W. M., Conway, T. M., Henderson, G. M., van Hulten,

924 M., Jeandel, C., Severmann, S., and Tagliabue, A.: Quantifying trace element and isotope

925 fluxes at the ocean–sediment boundary: a review, Philos Trans A Math Phys Eng Sci, 374,

926 2016.

927 Hutchins, D. A. and Bruland, K. W.: Grazer-mediated regeneration and assimilation of Fe, Zn

928 and Mn from planktonic prey, Mar. Ecol.-Prog. Ser., 110, 259-269, 1994.

929 Iwade, S., Kuma, K., Isoda, Y., Yoshida, M., Kudo, I., Nishioka, J., and Suzuki, K.: Effect of

930 high iron concentrations on iron uptake and growth of a coastal diatom Chaetoceros sociale,

931 Aquat. Microb. Ecol., 43, 177-191, 2006.

932 Jones, E. M., Bakker, D. C. E., Venables, H. J., and Hardman-Mountford, N. J.: Seasonal

933 cycle of CO2 from the sea ice edge to island blooms in the Scotia Sea, Southern Ocean, Mar.

934 Chem., 177, 490-500, 2015.

935 Jones, E. M., Bakker, D. C. E., Venables, H. J., and Watson, A. J.: Dynamic seasonal cycling

936 of inorganic carbon downstream of South Georgia, Southern Ocean, Deep-Sea Res. II, 59–60,

937 25-35, 2012.

938 Kalnejais, L. H., Martin, W. R., and Bothner, M. H.: The release of dissolved nutrients and

939 metals from coastal sediments due to resuspension, Mar. Chem., 121, 224-235, 2010.

940 Klar, J. K., Homoky, W. B., Statham, P. J., Birchill, A. J., Harris, E. L., Woodward, E. M. S.,

941 Silburn, B., Cooper, M. J., James, R. H., Connelly, D. P., Chever, F., Lichtschlag, A., and

942 Graves, C.: Stability of dissolved and soluble Fe(II) in shelf sediment pore waters and release

943 to an oxic water column, Biogeochemistry, 2017. 1-19, 2017.

944 Korb, R. E., Whitehouse, M. J., and Ward, P.: SeaWiFS in the southern ocean: spatial and

945 temporal variability in phytoplankton biomass around South Georgia, Deep-Sea Res. II, 51,

946 99-116, 2004.

947 Koschinsky, A., Winkler, A., and Fritsche, U.: Importance of different types of marine

948 particles for the scavenging of heavy metals in the deep-sea bottom water, Appl Geochem,

949 18, 693-710, 2003.

950 Kurapov, A. L., Allen, J. S., and Egbert, G. D.: Combined Effects of Wind-Driven Upwelling

951 and Internal Tide on the Continental Shelf, Journal of Physical Oceanography, 40, 737-756,

952 2010.

953 Lam, P. J. and Bishop, J. K. B.: The continental margin is a key source of iron to the HNLC

954 North Pacific Ocean, Geophys. Res. Lett., 35, 1-5, 2008.

955 Liu, X. and Millero, F. J.: The solubility of iron in seawater, Mar. Chem., 77, 43-54, 2002.

956 Ma, S., Tao, Z., Yang, X., Yu, Y., Zhou, X., M, W., and Li, Z.: Estimation of marine primary

957 productivity from satellite-derived phytoplankton absorption data, IEEE J-STARS, 7, 3084-

958 3092, 2014.

959 Marchetti, A., Parker, M. S., Moccia, L. P., Lin, E. O., Arrieta, A. L., Ribalet, F., Murphy, M.

960 E. P., Maldonado, M. T., and Armbrust, E. V.: Ferritin is used for iron storage in bloom-

961 forming marine pennate diatoms, Nature, 457, 467-470, 2009.

962 Marsay, C. M., Sedwick, P. N., Dinniman, M. S., Barrett, P. M., Mack, S. L., and

963 McGillicuddy, D. J.: Estimating the benthic efflux of dissolved iron on the Ross Sea

964 continental shelf, Geophys. Res. Lett., 41, 7576-7583, 2014.

965 Meredith, M. P., Brandon, M. A., Murphy, E. J., Trathan, P. N., Thorpe, S. E., Bone, D. G.,

966 Chernyshkov, P. P., and Sushin, V. A.: Variability in hydrographic conditions to the east and

967 northwest of South Georgia, 1996–2001, J. Marine Syst., 53, 143-167, 2005.

968 Milne, A., Schlosser, C., Wake, B. D., Achterberg, E. P., Chance, R., Baker, A. R., Forryan,

969 A., and Lohan, M. C.: Particulate phases are key in controlling dissolved iron concentrations

970 in the (sub)tropical North Atlantic, Geophys. Res. Lett., 44, 2377-2387, 2017.

971 Moore, W. S.: Determining coastal mixing rates using radium isotopes, Cont. Shelf Res., 20,

972 1993-2007, 2000.

973 Murphy, E. J., Trathan, P. N., Watkins, J. L., Reid, K., Meredith, M. P., Forcada, J., Thorpe,

974 S. E., Johnston, N. M., and Rothery, P.: Climatically driven fluctuations in Southern Ocean

975 ecosystems, P ROY SOC B-BIOL SCI, 274, 3057-3067, 2007.

976 Nielsdóttir, M. C., Bibby, T. S., Moore, C. M., Hinz, D. J., Sanders, R., Whitehouse, M.,

977 Korb, R., and Achterberg, E. P.: Seasonal and spatial dynamics of iron availability in the

978 Scotia Sea, Mar. Chem., 130–131, 62-72, 2012.

979 Pakhomova, S. V., Hall, P. O. J., Kononets, M. Y., Rozanov, A. G., Tengberg, A., and

980 Vershinin, A. V.: Fluxes of iron and manganese across the sediment–water interface under

981 various redox conditions, Mar. Chem., 107, 319-331, 2007.

982 Planquette, H., Sanders, R., Statham, P. J., Morris, P. J., and Fones, G. R.: Fluxes of

983 particulate iron from the upper ocean around the Crozet Islands: A naturally iron-fertilized

984 environment in the Southern Ocean, Global Biogeochem. Cycles, 25, 1-12, 2011.

985 Planquette, H., Statham, P. J., Fones, G. R., Charette, M. A., Moore, C. M., Salter, I.,

986 Nedelec, F. H., Taylor, S. L., French, M., Baker, A. R., Mahowald, N., and Jickells, T. D.:

987 Dissolved iron in the vicinity of the Crozet Islands, Southern Ocean, Deep-Sea Res. II, 54,

988 1999-2019, 2007.

989   Pollard, R. T., Salter, I., Sanders, R. J., Lucas, M. I., Moore, C. M., Mills, R. A., Statham, P.

990   J., Allen, J. T., Baker, A. R., Bakker, D. C. E., Charette, M. A., Fielding, S., Fones, G. R.,

991   French, M., Hickman, A. E., Holland, R. J., Hughes, J. A., Jickells, T. D., Lampitt, R. S.,

992   Morris, P. J., Nedelec, F. H., Nielsdottir, M., Planquette, H., Popova, E. E., Poulton, A. J.,

993   Read, J. F., Seeyave, S., Smith, T., Stinchcombe, M., Taylor, S., Thomalla, S., Venables, H.

994   J., Williamson, R., and Zubkov, M. V.: Southern Ocean deep-water carbon export enhanced

995   by natural iron fertilization, Nature, 457, 577-580, 2009.

996   Raiswell, R., Benning, L. G., Tranter, M., and Tulaczyk, S.: Bioavailable iron in the Southern

997   Ocean: the significance of the iceberg conveyor belt, Geochemical Transactions, 9, 1-9, 2008.

998   Raiswell, R. and Canfield, D. E.: The Iron Biogeochemical Cycle Past and Present,

999   Geochemical Perspectives, 1, 1-2, 2012.

1000 Rapp, I., Schlosser, C., Rusiecka, D., Gledhill, M., and Achterberg, E. P.: Automated

1001 preconcentration of Fe, Zn, Cu, Ni, Cd, Pb, Co, and Mn in seawater with analysis using high-

1002 resolution sector field inductively-coupled plasma mass spectrometry, Anal. Chimi. Acta,

1003 976, 1-13, 2017.

1004 Ratnarajah, L., Lannuzel, D., Townsend, A. T., Meiners, K. M., Nicol, S., Friedlaender, A.

1005 S., and Bowie, A. R.: Physical speciation and solubility of iron from baleen whale faecal

1006 material, Mar. Chem., 2017. 2017.

1007 Sato, M., Takeda, S., and Furuya, K.: Iron regeneration and organic iron(III)-binding ligand

1008 production during in situ zooplankton grazing experiment, Mar. Chem., 106, 471-488, 2007.

1009 Schlosser, C., De La Rocha, C. L., and Croot, P. L.: Effects of iron surface adsorption and

1010 sample handling on iron solubility measurements, Mar. Chem., 127, 48-55, 2011.

1011 Schmidt, K., Atkinson, A., Steigenberger, S., Fielding, S., Lindsay, M. C. M., Pond, D. W.,

1012 Tarling, G. A., Klevjer, T. A., Allen, C. S., Nicol, S., and Achterberg, E. P.: Seabed foreaging

1013   by Antarctic krill: Implications for stock assessment, bentho-pelagic coupling, and the

1014   vertical transfer of iron, Limnol. Oceanogr., 56, 1411-1428, 2011.

1015   Schmidt, K., Schlosser, C., Atkinson, A., Fielding, S., Venables, H. J., Waluda, C. M., and

1016   Achterberg, E. P.: Zooplankton gut passage mobilises lithogenic iron for ocean productivity,

1017   Curr. Biol., 26, 1-7, 2016.

1018   Strzepek, R., Maldonado, M. T., Hunter, K. A., Frew, R. D., and Boyd, P. W.: Adaptive

1019   strategies by Southern Ocean phytoplankton to lessen iron limitation: Uptake of organically

1020   complexed iron and reduced cellular iron requirements, Limnol. Oceanogr., 56, 1983-2002,

1021   2011.

1022   Tagliabue, A., Sallee, J.-B., Bowie, A. R., Levy, M., Swart, S., and Boyd, P. W.: Surface-

1023   water iron supplies in the Southern Ocean sustained by deep winter mixing, Nat Geosci, 7,

1024   314-320, 2014.

1025   Tsuda, A., Saito, H., Machida, R. J., and Shimode, S.: Meso- and microzooplankton

1026   responses to an in situ iron fertilization experiment (SEEDS II) in the northwest subarctic

1027   Pacific, Deep-Sea Res. II, 56, 2767-2778, 2009.

1028   Wedepohl, K. H.: The composition of the continental crust, Geochim. Cosmochim. Act., 59,

1029   1217-1232, 1995.

1030   Wells, M. L., Mayer, L. M., Donard, O. F. X., Sierra, M. M. D., and Ackelson, S. G.: The

1031   Photolysis Of Colloidal Iron In The Oceans, Nature, 353, 248-250, 1991.

1032   Whitehouse, M. J., Korb, R. E., Atkinson, A., Thorpe, S. E., and Gordon, M.: Formation,

1033   transport and decay of an intense phytoplankton bloom within the High-Nutrient Low-

1034   Chlorophyll belt of the Southern Ocean, J. Marine Syst., 70, 150-167, 2008.

1035   Wing, S. R., Jack, L., Shatova, O., Leichter, J. J., Barr, D., Frew R. D., and Gault-Ringold,

1036   M.: Seabirds and marine mammals redistribute bioavailable iron in the Southern Ocean, Mar.

1037   Ecol. Prog. Ser., 510, 1-13, 2014.

1038   Wolanski, E. J. and Delesalle, B.: Upwelling by internal waves, Tahiti, French Polynesia,

1039   Cont. Shelf Res., 15, 357-368, 1995.

1040   Yoshida, M., Kuma, K., Iwade, S., Isoda, Y., Takata, H., and Yamada, M.: Effect of aging

1041   time on the availability of freshly precipitated ferric hydroxide to costal marine diatoms, Mar.

1042   Biol., 149, 379-392, 2006.

1043

Table 1: OTE-seawater samples: Fe, Mn, and Al concentrations determined for the dissolved (D) (0.2 µm) and the leachable particulate fraction (LP$_{UN}$) (total dissolvable – dissolved) of unfiltered seawater samples collected during JR247. Additional information covers sampling date, site (station) ID, event number and latitude + longitude.

Date	Site ID	Depth	Leach. Part. (nmol L^{-1})			Dissolved (nmol L^{-1})		
	Lat. & Lon.	(m)	LP$_{Un}$Fe	LP$_{Un}$Mn	LP$_{Un}$Al	DFe	DMn	DAl
04/01/2011	#9/10 (E95 & E97)	20	20.36	0.95	46.41	5.71	1.83	1.11
		50	15.18	0.42	40.86	3.19	1.88	2.27
	54.26°S, 35.35°W	100	9.86	0.23	20.43	1.55	0.92	2.07
		130	23.33	0.73	48.91	2.82	0.87	2.68
		150	23.71	0.43	46.95	2.35	1.03	0.12
		200	27.37	0.62	54.41	2.70	0.89	2.37
05/01/2011	#11/12 (E98 & E101)	20	4.05	0.38	6.68	2.19	0.41	3.57
		35	1.52	0.39	7.28	0.41	0.37	-
	54.62°S, 34.81°W	50	9.30	0.60	22.20	7.18	0.64	13.31
		75	1.28	0.31	7.85	0.77	0.35	4.56
		100	2.02	0.32	3.34	1.09	0.35	1.47
		150	1.55	0.38	3.18	1.10	0.45	-
		200	13.10	1.31	23.81	1.26	1.17	3.07
		300	8.62	0.70	23.25	1.06	0.55	-
		400	8.81	0.54	16.54	2.05	0.46	2.69
		500	4.51	0.41	11.41	0.72	0.38	0.76
		600	2.75	0.37	10.32	0.96	0.36	0.77
		700	4.81	0.41	16.85	0.82	0.35	-
06/01/2011	#13 (E105)	20	3.46	0.62	14.68	0.28	0.57	4.53
		35	1.00	0.33	7.17	0.10	0.28	2.64
	54.53°S, 35.27°W	50	7.09	0.71	22.62	1.26	0.57	5.77
		75	25.03	1.09	61.94	1.23	0.64	5.86
		100	34.06	1.30	87.43	0.82	0.74	4.08
07/01/2011	#14 (E113)	20	4.00	0.89	7.87	0.64	0.85	2.57

41

Date	Station	Depth						
		50	2.23	0.31	7.64	0.27	0.32	1.80
	54.56°S, 35.59°W	75	2.30	0.43	3.58	0.62	0.46	2.42
		100	2.26	0.44	3.34	0.35	0.46	0.46
		150	23.50	0.94	33.35	0.70	0.62	0.23
		200	82.26	2.12	103.11	2.69	0.77	2.31
08/01/2011	#15/16 (E119 & E129)	20	17.66	0.46	26.66	0.99	1.36	-
		35	16.60	0.30	13.37	0.96	1.27	-
	53.62°S, 36.34°W	50	16.30	0.23	18.49	1.21	1.40	-
		75	23.82	0.56	29.86	0.98	1.28	-
		100	8.49	0.10	10.50	0.73	0.56	-
		150	1.88	0.03	4.49	2.25	0.40	-
		200	2.72	0.02	1.40	0.63	0.44	2.87
		300	2.56	0.05	2.40	0.34	0.25	-
		400	3.75	0.02	5.28	0.48	0.30	1.17
		500	5.28	0.08	9.22	0.43	0.30	-
		600	5.50	0.09	11.45	0.53	0.28	1.63
		750	5.27	0.06	8.16	0.44	0.30	-
10/01/2011	#17 (E133)	20	10.92	0.22	7.43	2.31	1.20	3.76
		35	20.83	0.53	16.22	1.81	1.34	2.56
	53.90°S, 36.57°W	50	34.59	1.00	57.55	2.29	1.42	2.33
		75	118.25	2.18	64.36	4.21	1.86	2.19
		100	50.71	1.00	77.52	2.48	1.42	1.62
		150	112.28	2.23	86.09	3.39	1.41	0.86
11/01/2011	#18 (E138)	20	106.71	1.77	95.17	2.75	1.57	3.36
		35	83.53	0.00	100.32	1.97	1.33	2.44
	54.10°S, 36.25°W	50	9.67	0.00	18.23	0.74	0.85	-
		75	5.65	0.00	8.90	0.62	0.65	-
		100	4.50	0.08	23.65	1.25	0.48	5.18
		150	7.81	0.11	12.87	1.43	0.49	8.19
12/01/2011	#19/20 (E141 & E143)	20	60.19	2.11	54.29	1.46	1.71	5.30
		35	60.17	2.19	87.17	1.34	1.90	8.22
	53.54°S, 38.11°W	50	66.78	2.74	141.75	1.57	1.90	8.73
		75	71.69	1.78	79.19	1.61	2.13	11.45

		100	10.77	0.25	32.12	0.99	0.67	10.74
		150	5.43	0.13	31.35	1.84	0.92	12.00
		200	7.92	0.14	27.42	1.45	0.60	9.60
		400	5.35	0.00	23.61	1.61	0.45	18.44
		600	5.81	0.10	35.99	1.06	0.38	10.74
		800	4.26	0.13	35.67	1.07	0.36	11.95
13/01/2011	#21 (E151)	20	44.75	1.54	114.13	0.72	1.38	2.58
		35	39.99	1.82	73.37	0.77	0.94	2.29
	53.75°S, 38.98°W	50	48.57	2.03	94.66	1.24	1.36	1.91
		75	25.63	0.91	68.56	0.98	1.17	-
		100	64.06	1.91	114.03	2.33	1.32	1.51
		150	73.04	1.59	62.83	7.70	1.28	12.20

1048

1049 **Table 2: SAPS samples:** The particulate Fe (PFe), Mn (PMn), and Al (PAl) concentrations in the top

1050 150 m of the water column at the 14 sites visited during JR247. The particulate fraction, P, is the sum

1051 of leachable particulate (LP) and refractory particulate (RP). Because of low concentrations, the

1052 leachable particulate fraction is indicated in percent of the P fraction. Additional information covers

1053 sampling date, site (station) ID, event number, latitude and longitude, and water column depth.

1054 (Depths marked by * indicate that the polycarbonate filter was corrupted after retrieving the SAPS)

Date	Site ID	Depth	Particulate (nmol L^{-1})			Leach. Part. (% of P)		
	Lat. & Lon.	(m)	PFe	PMn	PAl	LPFe	LPMn	LPAl
25/12/2010	#1/2 (E22)	20	5.17	0.08	4.82	0.37	2.39	1.65
	53.70°S, 38.21°W	50*	9.12	0.14	7.91	0.27	2.61	1.47
	(322 m)	150*	76.61	1.09	66.91	6.26	2.74	4.65
26/12/2010	#3 (E31)	20	6.62	0.09	6.64	0.02	3.30	0.79
	53.85°S, 39.14°W	50	267.48	3.85	162.59	1.48	0.79	0.65
	(287 m)	150	4.36	0.06	4.26	0.07	1.55	1.93
31/12/2010	#4/5 (E72)	20	8.52	0.12	7.99	0.51	1.68	2.62
	53.49°S, 37.71°W	50	15.15	0.23	12.96	0.56	2.44	2.74
	(1917 m)	150	2.33	0.03	2.15	0.65	1.78	2.42
02/01/2011	#6 (E80)	20	85.74	1.11	59.05	1.60	2.28	4.50
	53.99°S, 36.37°W	50	17.76	0.24	8.87	-	-	-
	(208 m)	150	137.39	2.02	98.54	3.46	0.91	2.81
03/01/2011	#7/8 (E88)	20	1.95	0.02	0.87	0.13	2.97	4.99
	54.10°S, 35.46°W	50	1.67	0.02	0.92	0.08	4.35	4.24
	(330 m)	150	1.23	0.02	0.71	0.19	2.11	5.13
04/01/2011	#9/10 (E96)	20	20.91	0.08	15.74	0.56	5.01	3.24
	54.26°S, 35.35°W	50	19.16	0.27	15.58	0.45	1.22	2.51
	(263 m)	150	54.06	0.77	48.10	1.08	1.65	2.08
05/01/2011	#11/12 (E100)	20*	1.49	0.01	0.86	0.18	4.42	2.92
	54.62°S, 34.81°W	50	0.87	0.01	0.60	0.27	6.63	4.20
	(747 m)	150	1.76	0.03	1.08	0.37	4.38	3.33
06/01/2011	#13 (E106)	20	2.75	0.03	1.78	0.63	3.13	4.29

|							
	54.53°S, 35.27°W	50	4.11	0.05	3.07	0.44	2.04	2.76
	(133 m)	100	10.28	0.15	7.62	0.46	1.70	2.54
07/01/2011	#14 (E114)	20	2.80	0.04	1.84	0.07	1.58	3.29
	54.56°S, 35.59°W	50	1.41	0.02	0.97	0.10	2.57	3.92
	(263 m)	150	31.34	0.46	26.92	0.72	1.57	2.28
08/01/2011	#15/16 (E120)	20	24.54	0.37	22.91	0.85	3.95	1.88
	53.62°S, 36.34°W	50	27.72	0.40	23.23	0.43	3.65	1.36
	(852 m)	150	4.74	0.07	3.94	0.90	4.31	1.06
10/01/2011	#17 (E134)	20	10.43	0.14	8.09	0.34	1.66	2.41
	53.90°S, 36.57°W	50	43.04	0.60	38.79	1.34	1.07	1.67
	(209 m)	150	207.48	3.10	194.88	1.72	0.82	1.50
11/01/2011	#18 (E139)	20	95.52	1.32	88.39	1.39	1.82	1.93
	54.10°S, 36.25°W	50	37.43	0.52	35.33	1.16	1.29	1.85
	(276 m)	150	28.00	0.41	23.60	1.26	2.35	2.27
12/01/2011	#19/20 (E142)	20	97.60	1.52	97.10	0.16	1.66	0.33
	53.54°S, 38.11°W	50	90.96	1.42	92.89	0.39	1.98	0.80
	(1741 m)	150	7.41	0.12	6.37	0.74	8.25	2.75
13/01/2011	#21 (E152)	20	50.75	0.85	52.78	0.06	2.99	0.12
	53.75°S, 38.98°W	50	59.59	0.93	59.98	0.05	2.15	0.09
	(269 m)	150	153.48	2.34	89.63	3.14	1.10	2.94

1055

45

1056 **Table 3: <mark>Sediment core samples:</mark>** Particulate iron (SFe), aluminum (SAl), and manganese (SMn)

1057 concentrations in shelf sediments collected during JC055 in January and February 2011. Pore water

1058 data retrieved additionally from these three cores are listed for Fe (Fe_{PW}) and Mn (Mn_{PW}). Additional

1059 information are event number (MC…), latitude + longitude, and water column depth.

Station ID Lat. & Lon.	Depth (cm)	SFe (mol kg-1)	SAl (mol kg-1)	SMn (mmol kg-1)	Fe_{PW} (µmol kg-1)	Mn_{PW} (µmol kg-1)
#S1 (MC33)	0.5	0.58	1.77	11.56	3.01	2.29
54.16°S, 37.98°W	1.5	0.61	1.74	11.52	17.47	0.84
(257 m)	2.5	0.59	1.77	11.78	110.90	0.28
	3.5	0.6	1.86	12.05	106.24	0.53
	4.5	0.58	1.72	11.82	94.09	0.34
	5.5	0.59	1.86	12.04	82.79	0.27
	9	0.56	1.72	11.19	32.98	0.00
	15	0.55	1.74	11.15	2.44	0.06
	25	0.53	1.6	10.81	0.80	0.16
#S2 (MC34)	0.5	0.64	1.77	11.42	1.53	0.87
54.16°S, 37.94°W	1.5	0.6	1.79	11.73	/	/
(247 m)	2.5	0.58	1.76	11.81	0.97	0.24
	6.5	0.59	1.83	12.23	11.19	0.26
	10.5	0.58	1.8	11.78	14.28	0.25
	14.5	0.54	1.6	10.83	3.59	0.33
	16.5	0.56	1.72	11.22	2.27	0.31
#S3 (MC35)	0.5	0.61	1.67	11.42	1.46	0.43
54.15°S, 37.97°W	1.5	0.59	1.76	11.7	28.94	0.35
(254 m)	2.5	0.58	1.76	11.7	91.52	0.37
	3.5	0.59	1.81	12.03	40.16	0.44
	5.5	0.57	1.78	11.58	49.37	0.56
	8.5	0.59	1.82	11.65	67.92	0.52
	17	0.54	1.69	10.8	3.87	0.34
	19	0.55	1.67	10.86	1.82	0.12
	25	0.55	1.77	11.19	2.73	0.36
	29	0.56	1.79	11.19	5.64	0.16

1060

1061   **Table 4: Krill faecal pellets:** Particulate (P) and leachable particulate (LP) concentrations for Fe,

1062   Mn, and Al determined for the 27 individual krill faecal pellet samples collected during 9 krill

1063   incubation experiments on-board RRS *James Clark Ross* (JR247). The particulate fraction, P, is the

1064   sum of leachable particulate (LP) and refractory particulate (RP). Because of low concentrations, the

1065   leachable particulate fraction of the faecal pellets is indicated in percent of the P fraction.

# Sample	pellet weight (mg)	PFe (μg mg^{-1})	PAl (μg mg^{-1})	PMn (ng mg^{-1})	LPFe (%)	LPAl (%)	LPMn (%)
1	4.87	0.88	1.06	12.5	6.33	8.83	13.24
2	2.18	1.33	1.68	16.7	3.02	8.81	8.22
3	4.26	1.07	1.90	17.8	5.37	3.27	11.81
4	1.91	5.19	5.53	76.1	2.15	1.95	5.68
5	1.41	2.70	2.84	39.1	2.46	1.59	3.54
7	7.80	67.1	64.2	998.3	2.93	2.21	3.25
8	0.99	2.71	2.42	35.0	3.76	4.59	5.99
10	1.48	6.42	4.89	71.6	0.29	4.83	0.91
13	2.79	4.13	3.11	50.3	0.36	5.07	1.53
15	0.77	37.3	38.1	531.1	2.03	2.80	6.21
16	1.21	6.35	6.22	81.2	1.24	7.47	3.13
18	12.27	40.0	36.6	582.5	3.95	2.07	4.29
19	2.19	11.2	9.49	146.9	0.15	2.03	1.07
22	2.43	48.1	49.7	721.5	0.81	2.32	0.98
40	3.35	22.8	22.0	337.4	5.51	3.21	5.50
41	8.55	6.91	7.14	103.1	1.11	1.88	4.31
42	3.5	25.7	24.8	376.2	5.09	2.98	5.29
45	0.40	3.96	4.43	43.3	1.27	13.90	1.46
47	7.65	3.63	3.92	52.7	0.34	0.68	3.65
48	0.63	3.06	3.21	34.1	0.05	4.22	0.76
49	4.42	29.6	28.5	438.4	1.65	2.93	1.95
50	7.46	2.31	2.37	34.6	0.36	0.51	2.78
51	5.18	28.0	27.1	431.3	1.85	2.60	2.01
62	1.20	4.63	4.68	68.0	0.31	1.78	0.47
68	2.25	44.0	40.2	667.4	4.84	1.95	4.77
69	1.66	43.6	44.8	663.7	5.66	2.13	5.46
71	3.47	35.3	36.4	557.7	1.50	1.99	1.76

1066
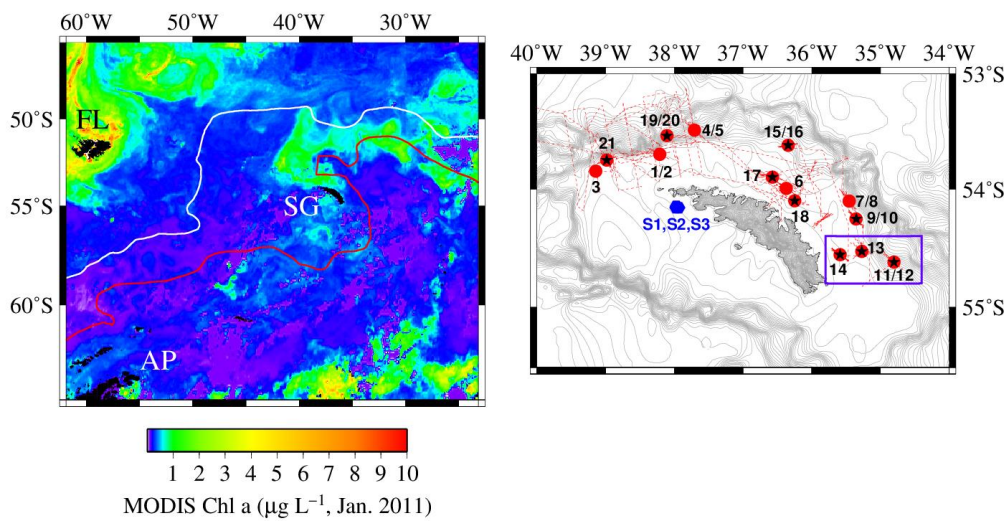
Figure 1: (Left figure) Locations of Falkland Islands (FL), South Georgia (SG), and Antarctic

Peninsula (AP) in the Atlantic sector of the Southern Ocean. South Georgia is located between the

Antarctic Polar Front (PF, white line) and the Subantarctic Circumpolar Current Front (SACCF, red

line). The colour bar represents the Chlorophyll a (Chl a) content recorded by the MODIS satellite in

January 2011. (Right figure) The region around SG and the **OTE** (black stars) and **SAPS** sampling

sites (red points) visited during JR247. The red dashed line illustrates the cruise track of JR247. The

three sediment sampling sites S1, S2, and S3 visited during JC055 are shown by blue hexagons. The

purple box indicates the W-E transect from shelf site #14 via site #13 to the shelf edge site #11/12.

The ocean bathymetry of the region was plotted using the GEBCO bathymetric data set. The shelf of

South Georgia is between 100 and 250 m deep and extends about 30 to 100 km (shelf edge indicated

by high density of isobaths).
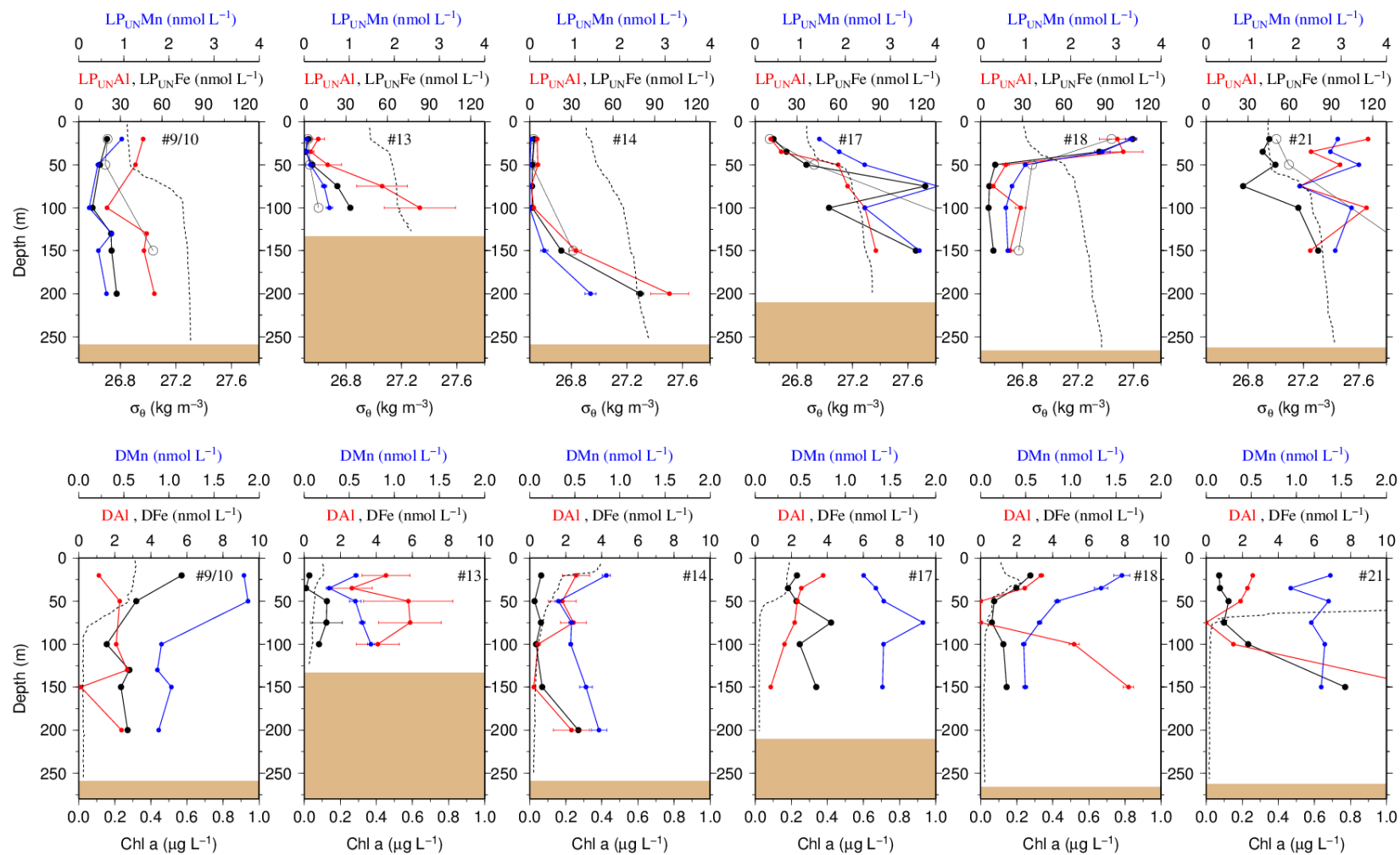
Figure 2: (Upper row) <mark>**OTE-seawater samples:**</mark> Distribution of leachable particulate iron ($LP_{Un}Fe$ in black), manganese ($LP_{Un}Mn$ in blue), and aluminium ($LP_{Un}Al$ in red) concentrations in the water column of stations located on the island shelf (125 m – 270 m water depth). <mark>**SAPS samples:**</mark> The particulate Fe (PFe) fraction retrieved by SAPS is illustrated with open black circles and corresponds to the concentration labels of $LP_{Un}Fe$. Concentrations above 120 nmol L^{-1} are listed in Table 1 and 2. Error bars represent the standard deviation of the analysis. Density sigma-theta (σ_θ) in kg m^{-3} is illustrated by the black dashed line. (Lower row) <mark>**OTE-seawater samples:**</mark> Dissolved iron (DFe), manganese (DMn), and aluminium (DAl) are represented by the same colour code as above. Dashed lines illustrate Chlorophyll a (Chl a) content of the water column recorded by the CTD fluorometer.
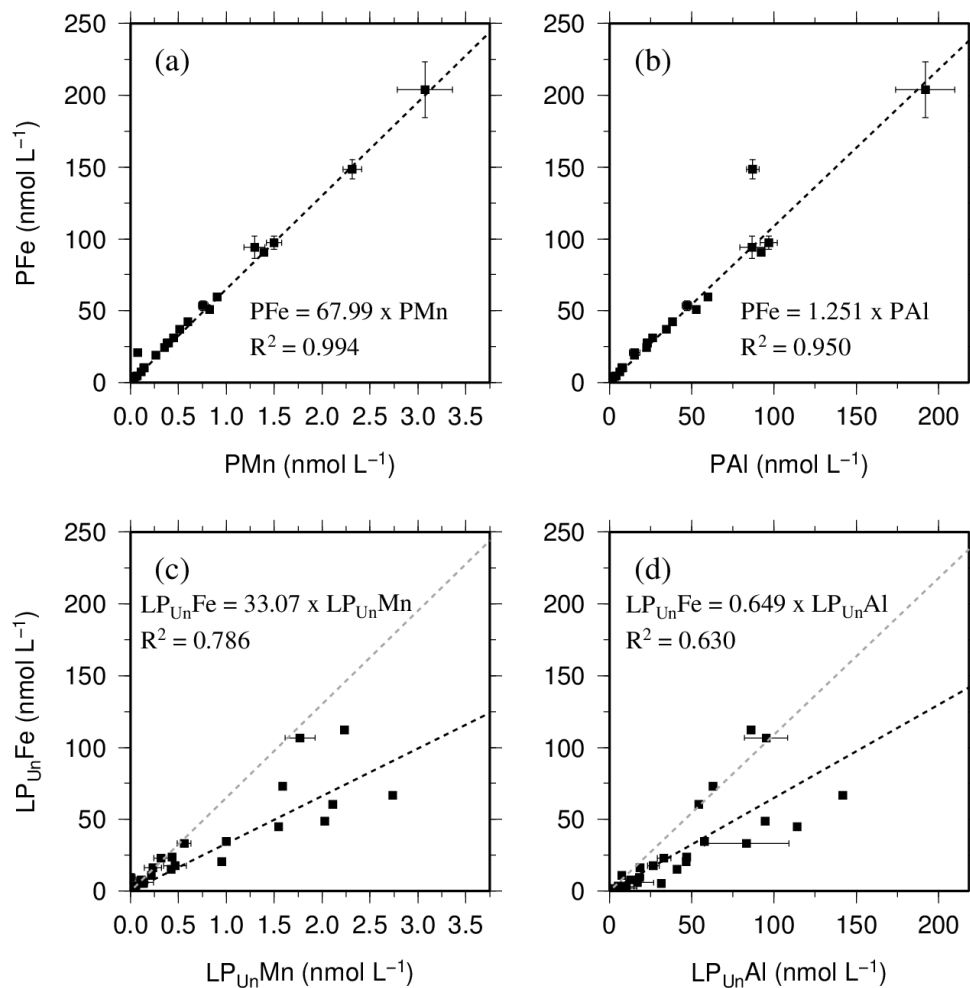
Figure 3: Relationship of the entire data set for the particulate fraction of Fe, Mn, and Al in particulates (P) retrieved using SAPS ((a) and (b)) and the leachable particulate fraction (LP_{UN}) estimated from unfiltered and dissolved seawater samples collected using OTE bottles ((c) and (d)). Error bars represent the standard deviation of the analysis. The linear regression of each relationship is illustrated by a dashed black line, the formula, and the R^2. The grey dashed line in c. and d. represents the linear relationship of particulate trace meals (P) shown in (a) and (b).
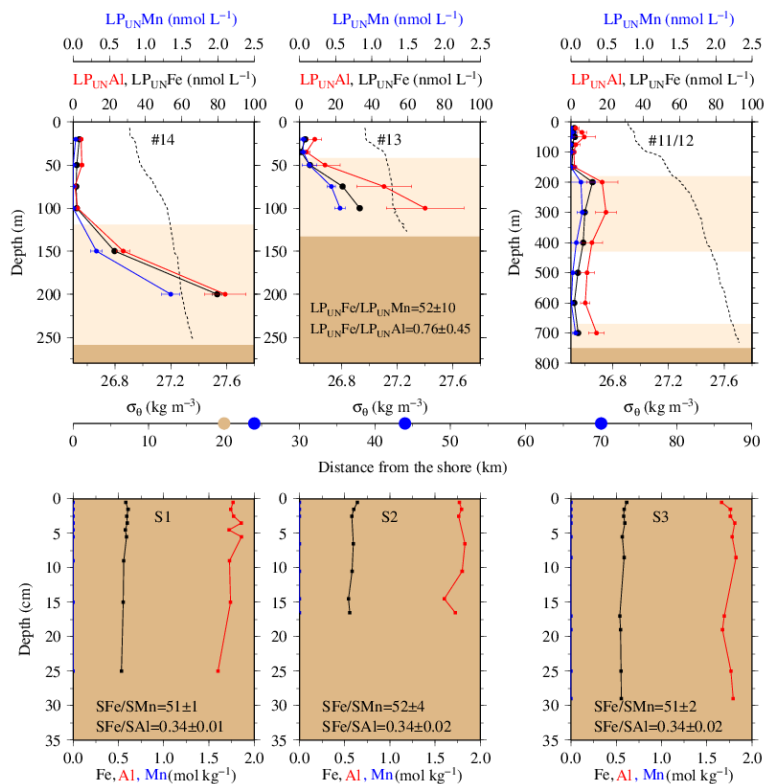
Figure 4: (Upper row) OTE-seawater samples: From left to right, concentrations of leachable particulate iron ($LP_{Un}Fe$), aluminium ($LP_{Un}Al$), and manganese ($LP_{Un}Mn$) of unfiltered seawater samples for the two shelf sites #14, #13 and the shelf edge site #11/12 (Note different depth scaling). Error bars represent the standard deviation of the analysis. Water density (sigma-theta (σ_θ)) is shown by the dashed black line. Brown areas represent sediments and pink areas the zone of resuspended sediment particles in the water column. Diagram 14 (left) contains the average $LP_{Un}Fe/LP_{Un}Al$ and $LP_{Un}Fe/LP_{Un}Mn$ ratio of particles in seawater samples collected within the pink layers. (Lower row) Sediment core samples: Diagram S1, S2 and, S3 displays the Fe, Mn, and Al content in the three sediment cores. Shown are average SFe/SAl and SFe/SMn ratios (mol/mol) of particles from the surface layer for site S1, S2, and S3. Dots on the distance scaling in the middle represent the distance of each water column station (blue) and sediment core (brown) station to the nearest shore.

53
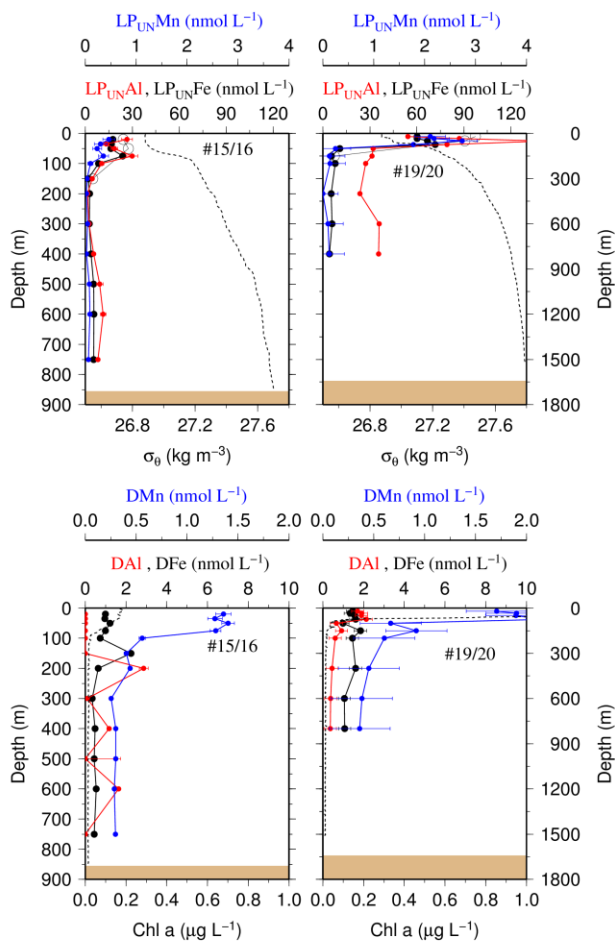
Figure 5: (Upper row) OTE-seawater samples: Distribution of leachable particulate manganese ($LP_{Un}Mn$ in blue), iron ($LP_{Un}Fe$ in black), and aluminium ($LP_{Un}Al$ in red) concentrations in the water column of the two other stations located on the island shelf edge (> 700 m water depth). SAPS samples: The particulate Fe (PFe) is illustrated by black circles and corresponds to the concentration labels of $LP_{Un}Fe$. Error bars represent the standard deviation of the analysis. Sigma-theta (σ_θ) is illustrated by the black dashed line. (Lower row) OTE-seawater samples: Dissolved manganese (DMn), iron (DFe), and aluminium (DAl) are represented by the same colour code as for the upper row. Dashed line illustrates the Chl a content of the water column recorded by the CTD mounted fluorometer.

54
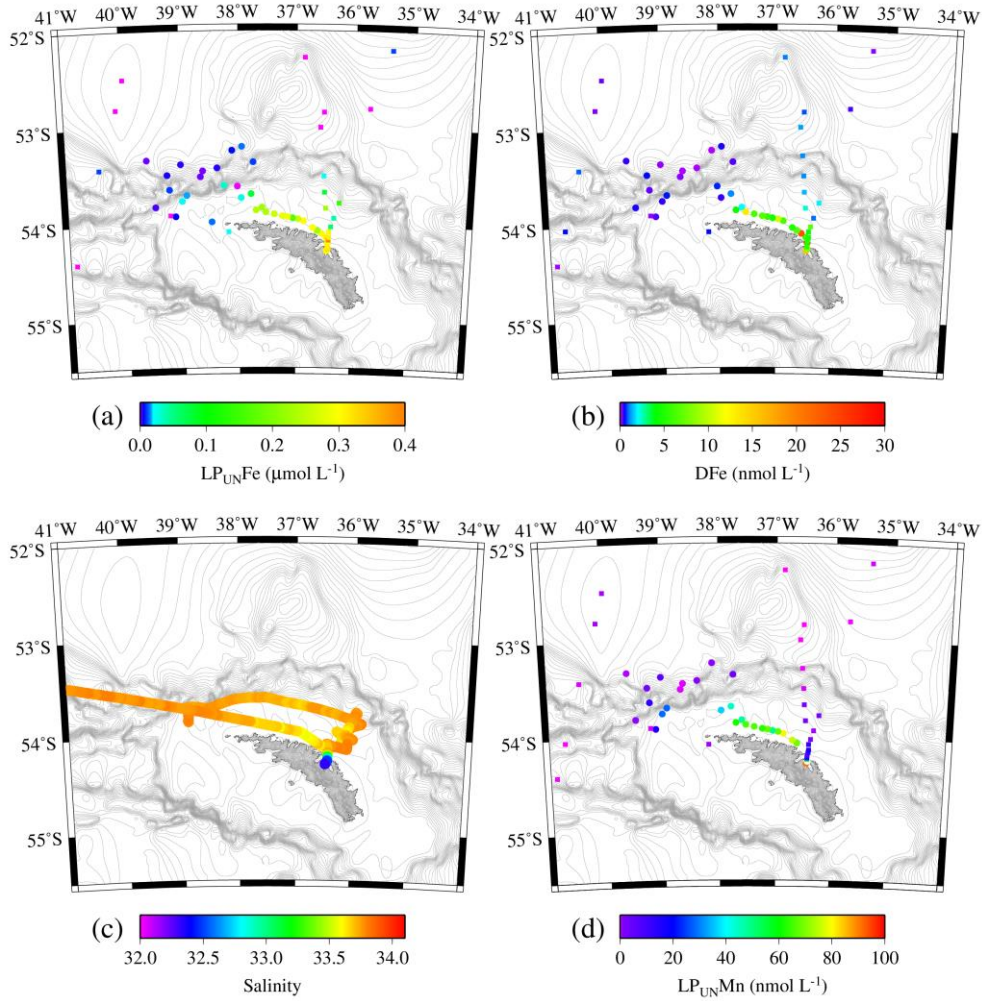
Figure 6: <mark>Tow fish-seawater samples:</mark> Concentrations of leachable particulate Fe (LP$_{UN}$Fe) of unfiltered seawater samples (a), dissolved Fe (DFe) (b), Salinity (c) and leachable particulate Mn (LP$_{UN}$Mn) in unfiltered seawater samples (d) in surface waters collected during JR247 (circles) and JR274 (squares) around South Georgia. <mark>The highest LP$_{UN}$Fe concentration was recorded in a single sample in Cumberland Bay reaching 2.2 µmol L^{-1}. Because of generally lower concentrations we excluded this data point in panel (a).</mark> Isobath are represented by grey lines (GEBCO – Gridded Bathymetry Data).
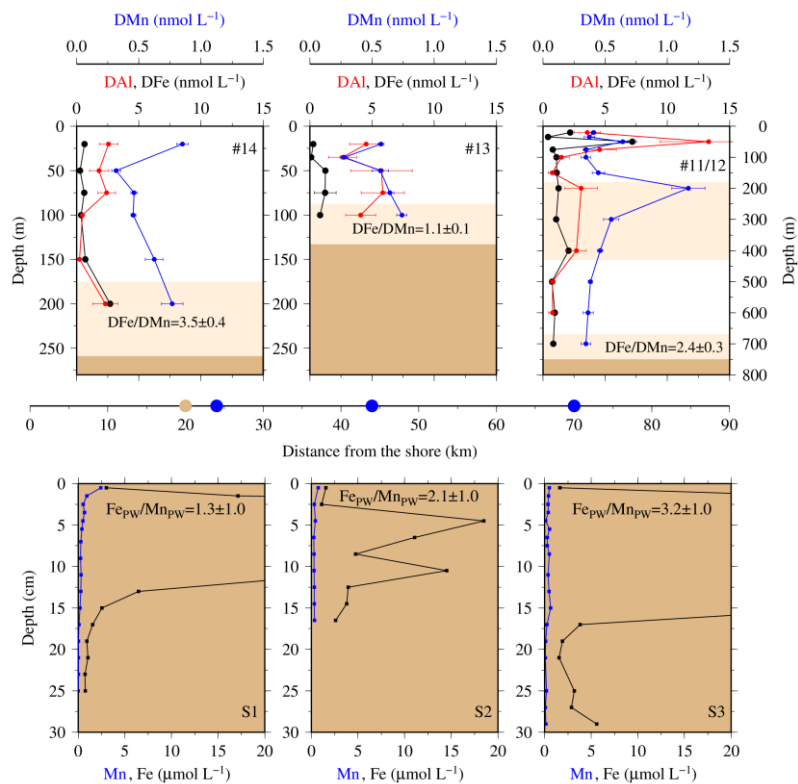
Figure 7: (Upper row) OTE-seawater samples: From left to right, concentrations of dissolved iron (DFe), aluminium (DAl), and manganese (DMn) for the two shelf sites (#14, #13) and the shelf edge site (#11/12). Note different depth scaling. Error bars represent the standard deviation of the analysis. Pink areas represent the zone of resuspended sediments in the water column. The DFe/DMn ratios of the seawaters collected within the pink zone is indicated. (Lower row) Sediment core samples: Diagram S1, S2 and, S3 displays the Fe (black), and Mn (blue) content in pore waters of the three sediment cores. Values off-axis can be found in Table 3. Shown are average Fe_{PW}/Mn_{PW} ratios (mol/mol) of top surface layer (1 cm) for site S1, S2, and S3. Dots on the distance scaling in the middle represent the distance of each water column station (blue) and sediment core (brown) station to the nearest shore.

56
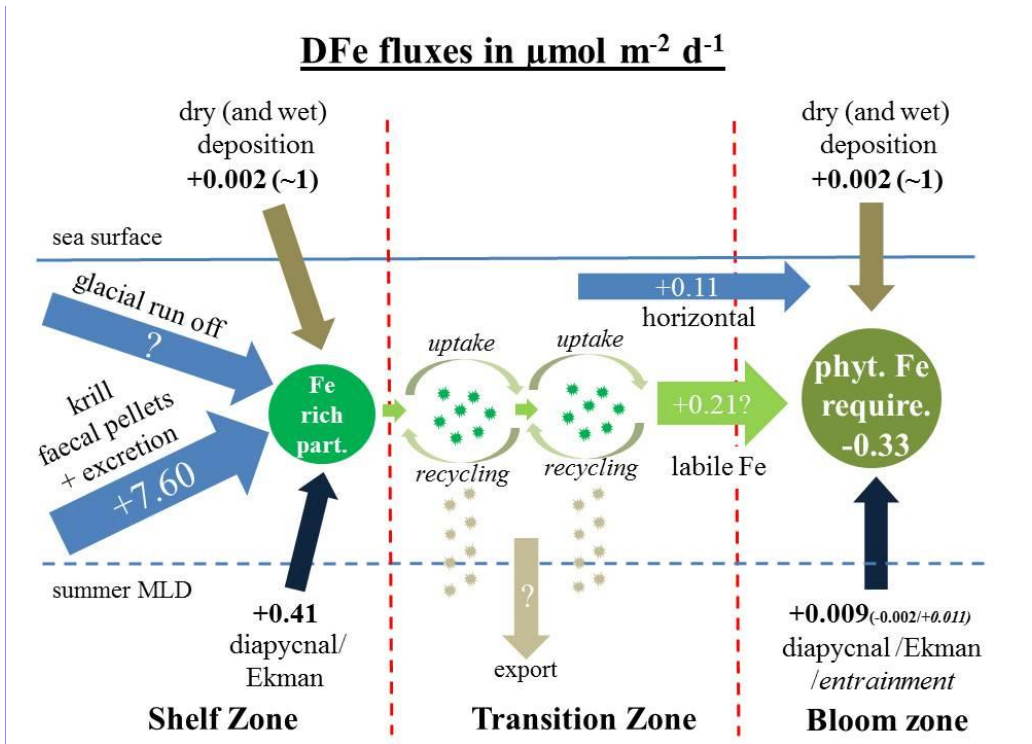
DFe fluxes in µmol m^{-2} d^{-1}

Figure 8: Sketch of DFe fluxes on the shelf, in the transition zone and in the downstream blooming region, separated by the red dashed lines. (left sketch) Describes the dissolved Fe fluxes on the shelf that together generate Fe rich biogenic and lithogenic particles (dark green). These are transferred offshore (light green arrows) following the ACC to open ocean sites (sketch in the middle). Iron enriched particles (dark green) in the transition zone are recycled and supplement DFe requirements of the phytoplankton community in the transition zone. During each cycle of recycling and uptake an unknown Fe fraction is lost by vertical export. (right sketch) Describes the dissolved Fe fluxes in the blooming zone.

Supplementary Material of

Mechanisms of dissolved and labile particulate iron supply to shelf waters and phytoplankton blooms off South Georgia, Southern Ocean

Christian Schlosser, Katrin Schmidt, Alfred Aquilina, William B. Homoky, Maxi Castrillejo, Rachel A. Mills, Matthew D. Patey, Sophie Fielding, Angus Atkinson, and Eric P. Achterberg

Supplementary Text

Text S1: Seawater sampling and analysis

Water column samples were collected using trace metal clean OTE bottles deployed on a Kevlar line. The OTE bottles were transferred into the clean container where all sample handling was performed. Dissolved and total dissolvable seawater samples were acidified immediately with concentrated trace metal grade nitric acid (HNO_3, UpA, Romil) to pH 1.66 (22 mmol H^+ L^{-1}). Acidified seawater samples were shipped to the National Oceanography Centre Southampton and analyzed by isotope dilution (ID) and standard addition inductively coupled plasma - mass spectrometry (ICP-MS).

The preconcentration and ICP-MS analysis was adapted from the method outlined by Rapp et al. (2017). Approximately one year after collection, 12 mL of acidified seawater was transferred into 30 mL fluorinated ethylene propylene (FEP) bottles and spiked with a spike solution containing mainly the artificially enriched isotope of iron (^{57}Fe). For the analysis of Al, and Mn a series of four standard additions were performed on every tenth sample. To obtain equimolar conditions between the spike and the natural seawater concentration, larger amounts of spike was added to the total dissolvable seawater samples. All samples were irradiated with strong ultraviolet light for 3.5 hours. Subsequently, the sample solution was buffered to pH 6.4 using a 2 M ammonium acetate solution (pH9.2, Fisher Optima grade

ammonia and acetic acid, glacial). Immediately after buffer addition the solution was preconcentrated using an automated system (Preplab, PS Analytical) that was equipped with a metal chelating resin (WACO) resin (Kagaya et al., 2009). Any remaining seawater salts were rinsed off using deionized water (> 18 MΩ cm, MilliQ, Millipore). The metals retained on the resin were eluted using 1 mL of a 1 M sub-boiled HNO_3 solution, which was collected in acid cleaned 4 mL polypropylene vials. The collected vials were placed into the auto-sampler of the ICP-MS (Element XR, Thermo).

The difference between the total dissolvable (TDM) and dissolved metal (DM) concentrations was used to determine the particulate concentration ($LP_{UN}M = TDM - DM$). It should be noted that this particulate fraction represents the amount of Fe ($LP_{UN}Fe$), Al ($LP_{UN}Al$), and Mn ($LP_{UN}Mn$) re-dissolved from particles within 1 year after the addition of 22 mmol H^+ L^{-1}. This means acid-inert minerals (e.g. zircon) and their associated trace metals likely did not contribute to the particulate metal concentration.

Certified seawater standards (SAFe D2 and GEOTRACES D) were preconcentrated and analyzed with each batch of samples, in order to validate our sample concentration. Values obtained by us for the certified seawater standards agreed with reported values for the GEOTRACES and the SAFe standard seawater (SAFe D2: 0.92 ± 0.02 nmol Fe L^{-1} (certified 0.90 ± 0.02 nmol Fe L^{-1}), GEOTRACES D: 1.00 ± 0.04 nmol Fe L^{-1} (certified 0.95 ± 0.05 nmol Fe L^{-1}). The precision for replicate analyses was between 1-3%. The buffer blank was $0.056 \pm 0.016(\sigma_{bl})$ nmol Fe L^{-1}, and the limit of detection (3 x standard deviation of the blank) was determined as $0.061 \pm 0.020(\sigma_{bl})$ nmol Fe L^{-1}.

Certified reference materials (crm), NIST 1573a and Tort 2, were digested and analysed with each batch of suspended particle and faecal pellet samples, in order to validate our sample concentration. Values obtained agreed with reported values of the crm (NIST 1573a: 423 ± 5 mg Fe kg^{-1} (certified 368 ± 7 mg Fe kg^{-1}), 244 ± 2 mg Mn kg^{-1} (certified 246 ± 8 mg Mn kg^{-1}), 550 ± 1 mg Al kg^{-1} (certified 598 ± 12 mg Al kg^{-1}); Tort-2: 117 ± 2 mg Fe kg^{-1} (certified 105 ± 13 mg Fe kg^{-1}), 13 ± 1 mg Mn kg^{-1} (certified 14 ± 1 mg Mn kg^{-1})).

Kommentar [SC27]: As requested by reviewer1, we included results from analysed crms

Text S2: Sediment and porewater sampling and analysis

Sediment cores with an undisturbed sediment-seawater interface were immediately transferred to a N_2-filled glove bag in a temperature-controlled laboratory to simulate ambient bottom water temperatures (approximately 4°C). Sediments were manually extruded at depth intervals of 1 or 2 cm into a polycarbonate ring, and sectioned using a polytetrafluoroethylene (PTFE) sheet that was cleaned with deionised water between each application. Porewater was separated from each sediment section by centrifugation at 9,000 g at 4°C under N_2 for 10 minutes; the supernatant porewaters were filtered under N_2 through 0.2 μm cellulose nitrate syringe filters (Whatman, UK). Aliquots of each porewater sample were collected in acid-cleaned LDPE bottles (Nalgene) and acidified to pH <2 by adding 2 μL of concentrated hydrochloric acid (HCl, UpA, Romil) per 1 mL of sample; acidified samples were stored refrigerated prior to analysis at NOCS. Conjugate sediments were freeze dried on board and stored at room temperature, pending analysis at the NOCS.

Sub-samples (~100 mg) of the bulk, homogenized sediments were completely dissolved using hot aqua regia (HNO_3+HCl) followed by hot hydrofluoric-perchloric acid (HF-$HClO_4$) mixtures and finally diluted in 0.6M HCl as described elsewhere (Homoky et al., 2011) . The acid digests were analysed by ICP-OES (Perkin Elmer Optima 4300DV). Calibration standards were matrix-matched and blank and instrument drift were monitored and corrected for by including calibration blanks and multi-element standards with each batch of 10 analyses. To ascertain the accuracy of the method certified reference material MAG-1 (United Sates Geological Survey) was analysed with each batch of samples. The values measured in our laboratory are in close agreement with the certified values: 42.978 ± 3.155 g Fe kg^{-1} (certified 47.600 ± 4.200 g Fe kg^{-1}); 715 ± 9 ng Mn g^{-1} (certified 760 ± 69 μg Mn kg^{-1}); and 76.605 ± 2.740 g Al kg^{-1} (certified 86.800 ± 1.600 g Al kg^{-1}).

Acidified porewater samples were analysed for a suite of major and trace elements, by ICP-OES (Perkin Elmer Optima 4300 DV). Elements including Fe and Mn were measured at 50-fold dilutions of the porewater sample in 0.6M HCl. Calibration standards were matrix matched and blank and instrument drift were monitored and corrected for by including calibration blanks

and multi-element standards for each batch of ten analyses. The instrument limits of detection (LD, 3 x standard deviation of acid blanks) were 1.25 µg Fe kg^{-1} and 0.08 µg Mn kg^{-1}.

Text S3: Calculation of dissolved Fe and Mn fluxes from shelf sediment porewaters

The calculation of pore water Fe and Mn fluxes follows the approach of Boudreux and Scott (1978), who described the flux of pore water Mn(II) by diffusion and reaction through an oxygenated surface layer in marine sediments.

$$J = \frac{\varphi(D_s k_1)^{0.5} C_p}{sinh((k_1/D_s)^{0.5} L)}$$

Where J is the flux (g cm^{-2} s^{-1}) of Mn(II) from sediment pore water to bottom water, L is the thickness (cm) of the oxygenated surface layer where Mn(II) is removed from the pore water by oxidative precipitation in the sediment, and C_p is the concentration (g cm^{-3}) of Mn(II) in the pore water beneath L relative to the overlying bottom water. The diffusive rate constant, D_s (cm^2 s^{-1}), is derived from sediment porosity (φ), and the Mn(II) oxidation rate constant, k_1 (s^{-1}), is estimated from field studies (Boudreux and Scott, 1978). This method has more recently been adopted for the determination of pore water Fe(II) fluxes (Homoky et al., 2013; Raiswell and Anderson, 2005) using the Fe(II) oxidation kinetics of (Millero et al., 1987) to derive k_1, and has been favourably compared with incubated flux determinations from shelf sediments (Homoky et al., 2012).

We use measured and estimated values for scalar terms for the flux calculations that are summarised in Supplementary Table S1 to investigate the potential for pore water fluxes of Fe and Mn from sites S1, S2 and S3. Sediment porosity (φ) was measured by the change in wet sediment mass after drying sliced core samples. Oxygen penetration depth (L) was measured from a single sediment core from site S3 with a Unisense microsensor apparatus following Homoky et al. (2013), and in the absence of multiple determinations is extrapolated to each core site. Diffusion coefficients (D_S) are a derived from measurements of φ after Boudreau and Scoot (1978). The oxidation rate constant (k_1) for Mn(II) is also

61

derived from Boudreau and Scoot (1978). For Fe(II), k_1 is calculated from values of bottom water O_2, temperature (0 °C), salinity (34) and an estimated pore water pH of 7.5 (Homoky et al., 2012), following Millero et al. (1987) (Homoky et al., 2013; Homoky et al., 2012; Raiswell and Anderson, 2005). Values of C_P are for measured data (at 0.5 and 1.5 cm depth) closest to the depth of L from each core site. Corresponding fluxes of pore water Fe (<0.1 to 44.4 μmol m^2 d^{-1}) and Mn (0.6 to 4.1 μmol m^2 d^{-1}) fall within the range of fluxes measured from continental margin sediments of the northeast Pacific (John et al., 2012; McManus et al., 2012) and demonstrate South Georgia shelf sediments are also likely to be an important source of Fe and Mn to the water column.

Text S4: Estimation of phytoplankton Fe requirements and Fe fluxes

The Fe requirements of the phytoplankton community within the bloom were estimated by combining satellite derived marine net primary productivity data (NPP = 62 ± 21 mmol C m^{-2} d^{-1} (Ma et al., 2014)) with an average intracellular Fe:C ratio (5.2 ± 2.8 μmol Fe mol^{-1} C^{-1} (Strzepek et al., 2011)). NPP was estimated from satellite-derived information using a phytoplankton pigment absorption based model (Ma et al., 2014). The applied NPP rate corresponded to an average chlorophyll a content in the euphotic zone of ~ 4 ug L^{-1}. There are several literature values for Fe:C ratio estimates ranging from 6 – 14 μmol Fe mol^{-1} C^{-1} under natural non Fe-fertilized and 10 – 40 μmol Fe mol^{-1} C^{-1} under Fe-fertilized conditions for Southern Ocean diatoms, autotrophic flagellates, and heterotrophic flagellates (Twining et al., 2004). Lab based incubation experiments using coastal phytoplankton species, such as *Dunaliella tertiolecta, Pyramimonas parkeae, Nannochloris atomus, Pycnococcus provasoli, Tetraselmis* sp.*, Gymnodinium chlorophorum, Prorocentrum mimimum, Amphidinium carterae, Thoracosphaera heimii, Emiliania huxleyia, Gephyrocapsa oceanica, Ditylum brightwellii, Thalassiosira weissflogii, Nitzschia brevirostris,*and *Thalassiosira eccentric*, reviled an average value of ~ 51 μmol Fe mol^{-1} C^{-1} (Ho et al., 2003), while Southern Ocean phytoplankton species including *Phaeocystis antarctica* (clone AA1), *Fragilariopsis kerguelensis, Thalassiosira Antarctica, Eucampia Antarctica*, and *Proboscia inermis* were an order of magnitude lower between 1.8 – 8.6 (Strzepek et al., 2011). Because most phytoplankton

species from the Southern Ocean are very well adapted to the very low Fe water content, we decided to apply the low Fe:C ratios provided by Strzepek et al. (Strzepek et al., 2011). The Fe:C ratio in the blooming region is presumingly higher, thus the rather low Fe:C ratio used refelcts the minimum amount of DFe that has to be supplied.

The vertical Fe flux (J_z) was calculated using an approach outlined in de Jong et al. (2012). The vertical DFe flux is the sum of advective Ekman pumping (left term) and diffusion (right term).

$$J_z = w[DFe]_{BWL} + K_z \left(\frac{\delta[DFe]}{\delta z} \right)$$

The advective Fe flux term (left) expressed by the upwelling velocity (w), which was set constant ~$1.1 * 10^{-6}$ m s^{-1} (de Jong et al., 2012), and the average dissolved Fe concentration ($[DFe]_{BWL}$) at all stations at ~ 200 m depth, contributed to 38% to the entire vertical Fe flux of 0.41 µmol m^{-2} d^{-1}. The remaining 62% are contribution of the diffusive mixing term (right term) which was derived from the DFe gradient at all stations between the surface mixed layer and ~ 200 m water depth and the vertical diffusivity, set constant at $K_z = 1 * 10^{-4} \, m^{-2} \, s^{-1}$.

Supplementary Tables

Table S1: Summary of pore water Fe and Mn flux parameters

| Parameter	Unit	--------------------- Fe ---------------------			--------------------- Mn ---------------------		
Site		S1	S2	S3	S1	S2	S3
Pore w. conc. C_p	(g cm^{-3})	1.7E-07 to 9.6E-07	6.2E-08 to 8.6E-08	9.2E-08 to 1.7E-06	4.9E-08 to 1.3E-07	1.8E-08 to 4.0E-08	2.2E-08 to 2.8E-08
O$_2$ depth, L	(cm)	0.7	0.7	0.7	0.7	0.7	0.7
Porosity, φ		0.76	0.76	0.84	0.76	0.76	0.84
Diff. coef., D_s	(cm^2 s^{-1})	2.076E-06	2.076E-06	2.461E-06	1.877E-06	1.877E-06	2.156E-06
Bottom water [O$_2$]	(g cm^{-3})	1.574E-05	1.574E-05	1.700E-05	1.00E-07	1.00E-07	1.00E-07
Pore water pH		7.5	7.5	7.5	7.5	7.5	7.5
Oxidation rate, k_1	(s^{-1})	1.574E-05	1.574E-05	1.700E-05	1.00E-07	1.00E-07	1.00E-07
Flux, J	(g cm^3 s^{-1})	2.2E-13 to 1.2E-12	4.3E-15 to 6.1E-15	1.6E-13 to 2.9E-12	1.0E-13 to 2.6E-13	3.6E-14 to 8.1E-14	5.8E-14 to 7.3E-14
	(μmol m^2 d^{-1})	3.4 to 19.2	<0.1	2.5 to 44.4	1.6 to 4.1	0.6 to 1.3	0.9 to 1.1

Table S2: <mark>Sediment core samples:</mark> Fe, Mn, and Al concentrations in pore waters and sediments

Date	Station	Sample ID	Sample mid-depth (cm)	Sediment particles Fe (wt %)	Mn (ppm)	Al (wt%)	Porewater Fe (μmol kg^{-1})	Mn (μmol kg^{-1})
Feb. 2011	S1 (MC33)	AC1	0.5	3.25	635	4.77	3.0	2.421
		AC2	1.5	3.38	633	4.70	17.2	0.940
		AC3	2.5	3.31	647	4.78	110.1	0.546
		AC4	3.5	3.35	662	5.01	105.6	0.675
		AC5	4.5	3.22	649	4.65	93.5	0.520
		AC6	5.5	3.30	662	5.02	81.9	0.389
		AD1	7	-	-	-	52.6	0.271
		AD2	9	3.11	615	4.66	32.6	0.263
		AD3	11	-	-	-	27.3	0.304
		AD4	13	-	-	-	6.4	0.293

		AD5	15	3.09	612	4.69	2.5	0.209
		AD6	17	-	-	-	1.4	0.087
		AE1	19	-	-	-	0.8	0.040
		AE2	21	-	-	-	0.8	0.027
		AE3	23	-	-	-	0.7	0.028
		AE4	25	2.99	594	4.31	0.7	0.008
Feb. 2011	S2 (MC34)	AF1	0.5	3.58	627	4.77	1.5	0.585
		AF2	1.5	3.35	644	4.83	-	-
		AF3	2.5	3.24	649	4.74	1.1	0.399
		AF5	4.5	-	-	-	18.5	0.304
		AG1	6.5	3.32	672	4.94	11.1	0.264
		AG3	8.5	-	-	-	4.7	0.253
		AG5	10.5	3.24	647	4.85	14.5	0.285
		AH1	12.5	-	-	-	3.9	0.290
		AH3	14.5	3.02	595	4.32	3.8	0.285
		AH5	16.5	3.11	616	4.65	2.6	0.336
Feb. 2011	S3 (MC35)	AI1	0.5	3.43	627	4.49	1.6	0.597
		AI2	1.5	3.28	643	4.75	29.0	0.465
		AI3	2.5	3.24	642	4.75	91.1	0.373
		AI4	3.5	3.32	661	4.88	40.2	0.342
		AI5	4.5	-	-	-	37.1	0.262
		AI6	5.5	3.16	636	4.81	49.3	0.535
		AJ1	6.5	-	-	-	37.4	0.251
		AJ2	7.5	-	-	-	61.7	0.322
		AJ3	8.5	3.27	640	4.92	67.9	0.475
		AJ4	11.0	-	-	-	48.2	0.398
		AJ5	13.0	-	-	-	23.6	0.336
		AJ6	15.0	-	-	-	33.5	0.648
		AK1	17.0	3.00	593	4.57	3.8	0.181
		AK2	19.0	3.05	597	4.51	1.9	0.075
		AK3	21.0	-	-	-	1.6	0.005
		AK5	25.0	3.08	615	4.77	3.2	0.071

AK6	27.0	-	-	-	2.9	0.052
AL1	29.0	3.10	615	4.83	5.6	0.095

Supplementary Figures
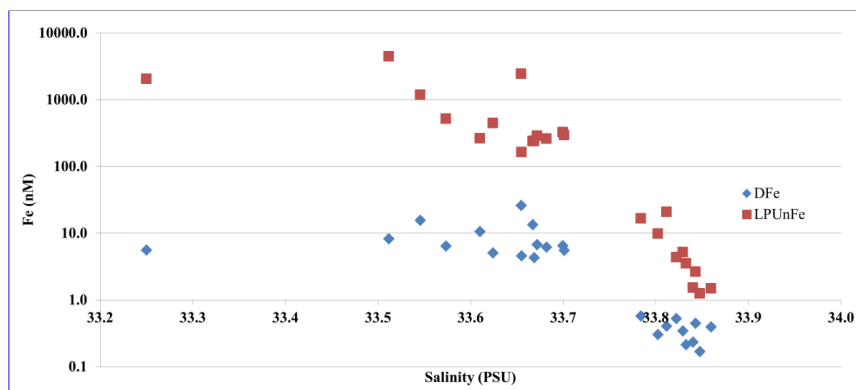
Figure S1: Tow-Fish surface samples: Relationship of salinity vs. dissolved (DFe) and leachable particulate Fe (LP$_{Un}$Fe) in surface waters. The Fe concentration along the y-axis is represented in a logarithmic scale. We applied a linear regression, to validate the relationship between the DFe, LP$_{Un}$Fe and salinity (not shown). With exception of the low salinity data point at 33.25 psu, the DFe and LP$_{Un}$Fe vs. salinity data achieved an R^2 of 0.46 and 0.38, respectively.
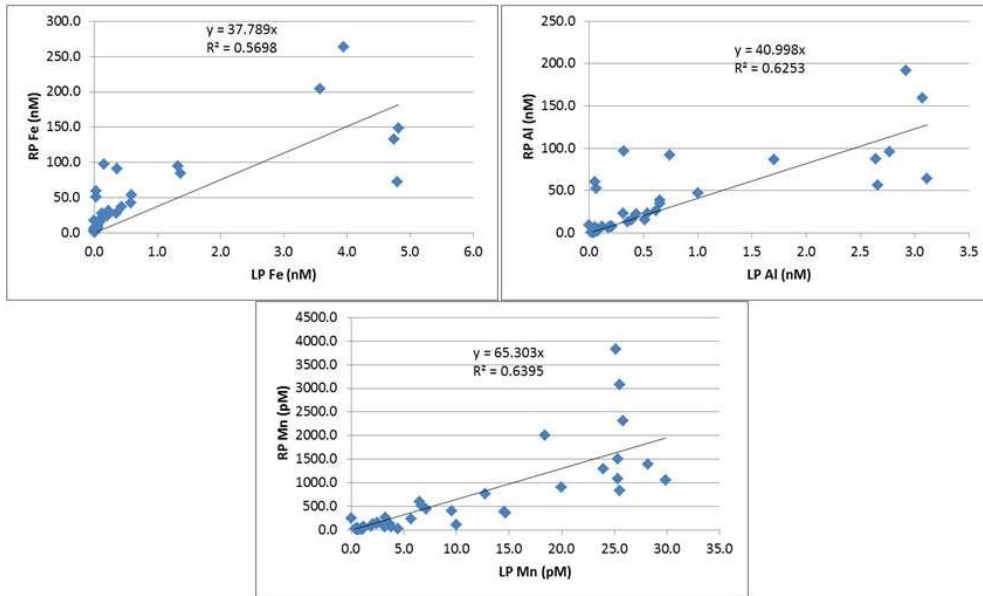
Figure S2: SAPS samples: Relationship between leachable particulate (LP) and refractory particulate (RP) Fe, Mn, and Al. Due to the high proportion of RP (98.9 – 99.2% for Fe) in the particulate fraction, using the particulate fraction, P, instead of RP changes the linear regression with LP just very little.
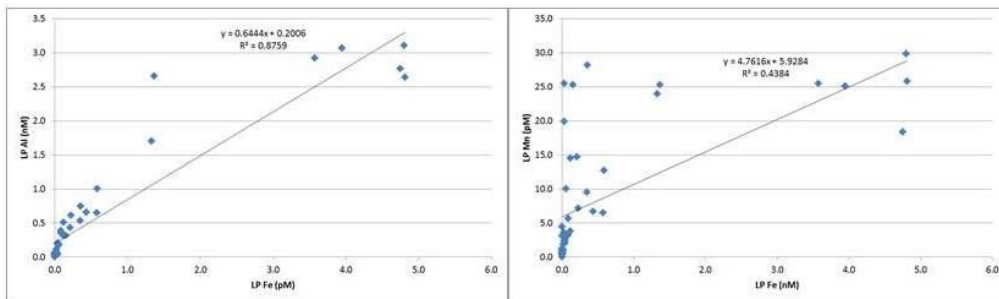
**Figure S3: SAPS samples :** Relationship between leachable particulate Fe, Mn and Al.
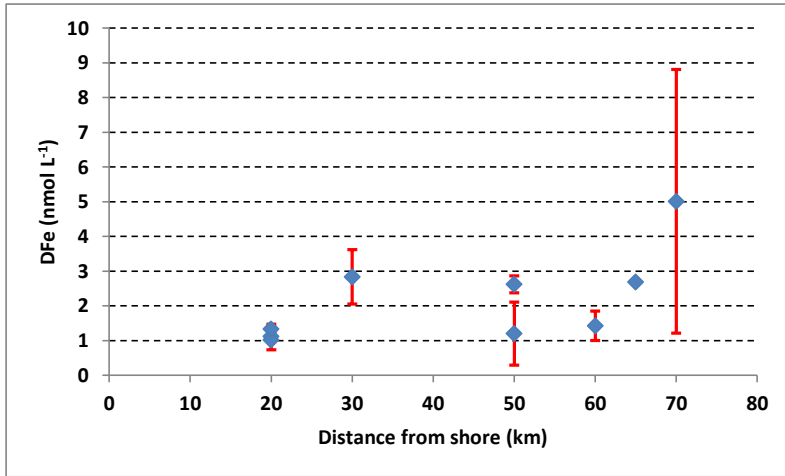
Figure S4: OTE-water sampler: Average dissolved Fe concentration between 100 and 400 m water depth versus distance to the coast line of South Georgia in kilometre.

References

Boudreux, B. P. and Scott, M. R.: A model for the diffusion-controlled growth of deep-sea manganese nodules, Americ. J. Sc., 278, 903-929, 1978.

de Jong, J., Schoemann, V., Lannuzel, D., Croot, P., de Baar, H. J. W., and Tison, J. L.: Natural iron fertilization of the Atlantic sector of the Southern Ocean by continental shelf sources of the Antarctic Peninsula, J. Geophys. Res., 117, 1-25, 2012.

Ho, T.-Y., Quigg, A., Finkel, Z. V., Milligan, A. J., Wyman, K., Falkowski, P. G., and Morel, F. M. M.: The elemental composition of some marine phytoplankton, J. Phycol., 39, 1145-1159, 2003.

Homoky, W. B., John, S. G., Conway, T. M., and Mills, R. A.: Distinct iron supply and isotope signatures from marine sediment dissolution, Nat. Commun., 4:2143, 2013.

Homoky, W. B., Severmann, S., McManus, J., Berelson, W. M., Riedel, T. E., Statham, P. J., and Mills, R. A.: Dissolved oxygen and suspended particles regulate the benthic flux of iron from continental margins, Mar. Chem., 134–135, 59-70, 2012.

John, S. G., Mendez, J., Moffett, J. W., and Adkins, J.: The flux of iron and iron isotopes from San Pedro Basin sediments, Geochim. Cosmochim. Act., 93, 14-29, 2012.

Kagaya, S., Maebe, E., Inoue, Y., Kamichatani, W., Kajiwara, T., Yanai, H., Saito, M., and Tohda, K.: A solid phase extraction using a chelate resin immobilizing carboxymethylated pentaethylenehexamine for separation and preconcentration of trace elements in water samples, Talanta, 79, 146-152, 2009.

Ma, S., Tao, Z., Yang, X., Yu, Y., Zhou, X., M, W., and Li, Z.: Estimation of marine primary productivity from satellite-derived phytoplankton absorption data, IEEE J-STARS, 7, 3084-3092, 2014.

McManus, J., Berelson, W. M., Severmann, S., Johnson, K. S., Hammond, D. E., Roy, M., and Coale, K. H.: Benthic manganese fluxes along the Oregon-California continental shelf and slope, Cont. Shelf Res., 43, 71-85, 2012.

Millero, F. J., Sotolongo, S., and Izaguirre, M.: The oxidation kinetics of Fe(II) in seawater, Geochim. Cosmochim. Act., 51, 793-801, 1987.

Raiswell, R. and Anderson, T. F.: Reactive iron enrichment in sediments deposited beneath euxinic bottom waters: constraints on supply by shelf recycling, Geological Society, London, Special Publications, 2005.

Rapp, I., Schlosser, C., Rusiecka, D., Gledhill, M., and Achterberg, E. P.: Automated preconcentration of Fe, Zn, Cu, Ni, Cd, Pb, Co, and Mn in seawater with analysis using high-resolution sector field inductively-coupled plasma mass spectrometry, Anal. Chimi. Acta, 976, 1-13, 2017.

Strzepek, R., Maldonado, M. T., Hunter, K. A., Frew, R. D., and Boyd, P. W.: Adaptive strategies by Southern Ocean phytoplankton to lessen iron limitation: Uptake of organically complexed iron and reduced cellular iron requirements, Limnol. Oceanogr., 56, 1983-2002, 2011.

Twining, B. S., Baines, S. B., Fisher, N. S., and Landry, M. R.: Cellular iron contents of plankton during the Southern Ocean Iron Experiment (SOFeX), Deep-Sea Res. I, 51, 1827-1850, 2004.